Inorg. Chem. **2008**, *47*, 9537−9552

Thermally Induced Magnetic Anomalies in Solvates of the Bis(hexafluoroacetylacetonate)copper(II) Complex with Pyrazolyl-Substituted Nitronyl Nitroxide

Victor I. Ovcharenko,* Galina V. Romanenko, Ksenia Yu. Maryunina, Artem S. Bogomyakov, and Elena V. Gorelik

International Tomography Center, Russian Academy of Sciences, Institutskaya Street 3A, Novosibirsk 630090, Russian Federation

Received June 18, 2008

We succeeded in synthesizing of a whole family of isostructural solvates of the copper(II) hexafluoroacetylacetonate complex with pyrazolyl-substituted nitronyl nitroxide (L): $Cu(hfac)_2L \cdot 0.5Solv$. The main feature inherent in nature of $Cu(hfac)_2L \cdot 0.5Solv$ single crystals is their incredible mechanical stability and ability to undergo reversible structural rearrangements with temperature variation, accompanied by anomalies on the $\mu_{eff}(T)$ dependence. Structural investigation of the complexes over a wide temperature range before and after the structural transition and the ensuing magnetic phase transition showed that the spatial peculiarities of the solvent molecules incorporated into the solid govern the character of the $\mu_{eff}(T)$ dependence and the temperature region of the magnetic anomaly. Thus, doping of crystals with definite solvent molecules could be used as an efficient method of control over the magnetic anomaly temperature (T_a). The investigation of this special series of crystals has revealed the relationship between the chemical step and the magnetic properties. It was shown that "mild" modification of T_a for $Cu(hfac)_2L \cdot 0.5Solv$ required a much smaller structural step than the typical change of one $-CH_2-$ fragment in a homologous series in organic chemistry. Quantum-chemical calculations with the use of X-ray diffraction data allowed us to trace the character of changes in the exchange interaction parameters in the range of the phase transition. In the temperature range of the phase transition, the exchange parameter changes substantially. The gradual decrease in the magnetic moment, observed in most experiments during sample cooling to T_a, is the result of the gradual increase in the fraction of the low-temperature phase in the high-temperature phase.

Introduction

Recently, so-called breathing crystals based on stereochemically nonrigid heterospin complexes of bis(hexafluoroacetylacetonato)copper(II) and nitronyl nitroxides have been discovered.[1] The key feature of these crystals is as follows. The thermally induced structural rearrangements of the $\{Cu^{II}-O^{\bullet}-N<\}$ or $\{>N-^{\bullet}O-Cu^{II}-O^{\bullet}-N<\}$ multispin exchange clusters provoke magnetic anomalies in their $\mu_{eff}(T)$ dependence, which are similar to the classical spin transitions.[2−4] However, as compared to classical cases, the source of these anomalies is principally new: *a strong change in the energy of exchange coupling between the odd electrons of paramagnetic centers*.[1a−j] The dynamics of the spin clusters shows itself specifically in the electron spin resonance (ESR) spectra of breathing crystals and allows us to obtain valuable details about the interactions of paramagnetic centers.[1k−n] Recently, for stereochemically nonrigid copper complexes with pyrazolyl-substituted derivatives of nitronyl nitroxides, it was shown that the magnetic anomalies might be accompanied by substantial changes in J, while the classical concept states that the exchange integral (J) is insensitive to variation of the temperature.[1m]

After the transition point, the single crystals of $Cu(hfac)_2$ complexes with pyrazolyl-substituted nitronyl nitroxides often retain their X-ray quality, which is an important peculiarity of these compounds.[1f−k] Because of this, one can trace the structure dynamics before and after the phase transition. Previously, it was shown that varying an alkyl substituent in the pyrazole fragment of the paramagnetic ligand considerably affected the structure of the solid

* To whom correspondence should be addressed. E-mail: Victor.Ovcharenko@tomo.nsc.ru.

10.1021/ic8011074 CCC: $40.75
Published on Web 09/10/2008

phase[1f−i] and hence the magnetic properties of the compounds. It was also reported that modification of coordination units by forming mixed-metal solid solutions was an effective method for changing the magnetic properties of compounds.[5] The temperature of the magnetic anomaly could also be varied within wide limits by forming solid solutions containing different paramagnetic ligands.[1i]

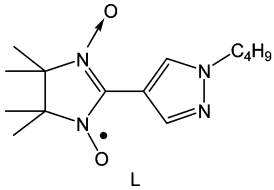

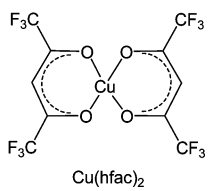

Quite unexpected results, however, were obtained when we tried to *control* the temperature and the type of magnetic anomaly in Cu(hfac)$_2$L$^{\bullet}$0.5Solv[1g,l] by varying the solvent molecules incorporated in the interchain space. The temperature and the type of magnetic anomaly in this case could only be affected by van der Waals interactions between the heterospin polymer chains and the incorporated solvent molecules; therefore, one could expect that variation of the solvent molecules lying in the interchain space, far away from the heterospin exchange clusters that undergo structural rearrangements, might have an insignificant effect on the magnetic anomaly temperature.

However, our investigation showed that variation of the low-polar solvate molecules in Cu(hfac)$_2$L$^{\bullet}$0.5Solv could substantially affect the magnetic anomaly temperature (T_a) and the character of the magnetic effect; i.e., it could serve as *a powerful tool for control over the magnetic anomaly*. It was also found that "mild" modification of T_a in Cu(hfac)$_2$L$^{\bullet}$0.5Solv required a considerably smaller structural step than that typical in the organic chemistry change of one methylene unit in the homologous series. The selective substitution of the solvent in Cu(hfac)$_2$L$^{\bullet}$0.5Solv (Solv = pentane, hexane, heptane, octane, octene, butyl chloride, butyl bromide, butyl iodide, amyl chloride, amyl bromide, amyl iodide) and further complete structure determination in different temperature ranges before and after the structural phase transition made it possible to analyze the atomic motions not only inside the coordination polyhedra but also in regions occupied by solvate molecules in crystals. The X-ray movie demonstrated mutual coherence between the structure dynamics of the >N−$^{\bullet}$O−Cu^{II}−O$^{\bullet}$−N< heterospin exchange clusters and the structure dynamics of the interchain diamagnetic fragments. These mutually coherent intra- and interchain atomic motions, which are responsible for the mechanical stability of crystals, determine the character of the structural rearrangement of the solid phase in general and the type of magnetic anomaly. Quantum-chemical analysis of the exchange interaction parameters based on the structural data for complexes at different temperatures revealed the character of changes in J(CuL) inside the >N−$^{\bullet}$O−Cu^{II}−O$^{\bullet}$−N< exchange clusters; these results, together with the data on the $\mu_{eff}(T)$ dependences, allowed us to draw the conclusion about the mechanism of the phase transition.

Experimental Section

Materials and Physical Techniques. All of the solvents were commercially available and used as received. Cu(hfac)$_2$L$^{\bullet}$0.5Solv complexes, where Solv is hexane, heptane, octane, and octene and L is the nitronyl nitroxide 2-(1-butyl-1*H*-pyrazol-4-yl)-4,4,5,5-tetramethyl-4,5-dihydro-1*H*-imidazole-3-oxide-1-oxyl, were prepared as described previously.[1g,l,6] Special care was taken to avoid solvent losses during the experiments. For the reasons described elsewhere,[1j] the same freshly prepared samples were used for X-ray diffraction experiment and measurements of $\chi(T)$. All measurements were carried out on an MPMS*XL* SQUID magnetometer (Quantum Design) in the temperature range 2−300 K and with a magnetic field of up to 5 kOe. Molar magnetic susceptibility was calculated

(1) (a) Lanfranc de Panthou, F.; Belorizky, E.; Calemczuk, R.; Luneau, D.; Marcenat, C.; Ressouche, E.; Turek, P.; Rey, P. *J. Am. Chem. Soc.* **1995**, *117*, 11247–11253. (b) Lanfranc de Panthou, F.; Luneau, D.; Musin, R.; Öhrström, L.; Grand, A.; Turek, P.; Rey, P. *Inorg. Chem.* **1996**, *35*, 3484–3491. (c) Iwahory, F.; Inoue, K.; Iwamura, H. *Mol. Cryst. Liq. Cryst.* **1999**, *334*, 533–538. (d) Caneschi, A.; Chiesi, P.; David, L.; Ferraro, F.; Gatteschi, D.; Sessoli, R. *Inorg. Chem.* **1993**, *32*, 1445–1453. (e) Baskett, M.; Lahti, P. M.; Paduan-Filho, A.; Oliveira, N. F., Jr. *Inorg. Chem.* **2005**, *44*, 6725–6735. (f) Ovcharenko, V. I.; Fokin, S. V.; Romanenko, G. V.; Shvedenkov, Yu. G.; Ikorskii, V. N.; Tretyakov, E. V.; Vasilevsky, S. F. *Russ. J. Struct. Chem. (Engl. Transl.)* **2002**, *43*, 153–169. (g) Ovcharenko, V. I.; Fokin, S. V.; Romanenko, G. V.; Ikorskii, V. N.; Tretyakov, E. V.; Vasilevsky, S. F.; Sagdeev, R. Z. *Mol. Phys.* **2002**, *100*, 1107–1115. (h) Rey, P.; Ovcharenko, V. I. In *Magnetism: Molecules to Materials, IV*; Miller, J. S., Drillon, M., Eds.; Wiley-VCH: New York, 2003; pp 41−63. (i) Ovcharenko, V. I.; Maryunina, K. Yu.; Fokin, S. V.; Tretyakov, E. V.; Romanenko, G. V.; Ikorskii, V. N. *Russ. Chem. Bull. (Engl. Transl.)* **2004**, *240*, 2406–2427. (j) Fokin, S.; Ovcharenko, V.; Romanenko, G.; Ikorskii, V. *Inorg. Chem.* **2004**, *43*, 969–977. (k) Fedin, M.; Veber, S.; Gromov, I.; Ovcharenko, V.; Sagdeev, R.; Bagryanskaya, E. *J. Phys. Chem. A* **2007**, *111*, 4449–4455. (l) Fedin, M.; Veber, S.; Gromov, I.; Maryunina, K.; Fokin, S.; Romanenko, G.; Sagdeev, R.; Ovcharenko, V.; Bagryanskaya, E. *Inorg. Chem.* **2007**, *46*, 11405–11415. (m) Veber, S. L.; Fedin, M. V.; Potapov, A. I.; Maryunina, K. Yu.; Romanenko, G. V.; Sagdeev, R. Z.; Ovcharenko, V. I.; Goldfarb, D.; Bagryanskaya, E. G. *J. Am. Chem. Soc.* **2008**, *130*, 2444–2445. (n) Fedin, M.; Veber, S.; Gromov, I.; Ovcharenko, V.; Sagdeev, R.; Schweiger, A.; Bagryanskaya, E. *J. Phys. Chem. A* **2006**, *110*, 2315–2317.

(2) (a) Sorai, M.; Ensling, J.; Hasselbach, K. M.; Gütlich, P. *Chem. Phys.* **1977**, *20*, 197–208. (b) Gütlich, P.; Köppen, H.; Steinhäuser, H. G. *Chem. Phys. Lett.* **1980**, *74*, 475–480. (c) Gütlich, P.; Hauser, A.; Spiering, H. *Angew. Chem., Int. Ed. Engl.* **1994**, *33*, 2024–2054. (d) Murray, K. S.; Kepert, C. J. In *Topics in Current Chemistry*; Gütlich, P., Goodwin, H. A., Eds.; Springer-Verlag: Berlin, 2004; Vol. *233*, pp 216−219. (e) Sorai, M. In *Topics in Current Chemistry*; Gütlich, P., Goodwin, H. A., Eds.; Springer-Verlag: Berlin, 2004; Vol. *235*, pp 151−161.

(3) (a) Katz, B. A.; Strouse, C. E. *J. Am. Chem. Soc.* **1979**, *101*, 6214–6221. (b) Mikami, M.; Konno, M.; Saito, Y. *Chem. Phys. Lett.* **1979**, *63*, 566–569. (c) Greenaway, A. M.; Sinn, E. *J. Am. Chem. Soc.* **1978**, *100*, 8080–8084. (d) Greenaway, A. M.; O'Connor, C. J.; Schrock, A.; Sinn, E. *Inorg. Chem.* **1979**, *18*, 2692–2695. (e) Wiehl, L.; Kiel, G.; Köhler, C. P.; Spiering, H.; Gütlich, P. *Inorg. Chem.* **1986**, *25*, 1565–1571.

(4) (a) Cecconi, F.; Di Vaira, M.; Midollini, S.; Orlandini, A.; Sacconi, L. *Inorg. Chem.* **1981**, *20*, 3423–3430. (b) Hostettler, M.; Törnroos, K. W.; Chernyshov, D.; Vangdal, B.; Bürgi, H.-B. *Angew. Chem., Int. Ed.* **2004**, *43*, 4589–4594. (c) Halder, G. J.; Kepert, C. J.; Moubaraki, B.; Murray, K. S.; Cashion, J. D. *Science* **2002**, *298*, 1762–1765. (d) Törnroos, K. W.; Hostettler, M.; Chernyshov, D.; Vangdal, B.; Bürgi, H.-B. *Chem. Eur. J.* **2006**, *12*, 6207–6215. (e) Neville, S. M.; Halder, G. J.; Chapman, K. W.; Duriska, M. B.; Southon, P. D.; Cashion, J. D.; Létard, J.-F.; Moubaraki, B.; Murray, K. S.; Kepert, C. J. *J. Am. Chem. Soc.* **2008**, *130*, 2869–2876.

(5) Maryunina, K.; Fokin, S.; Ovcharenko, V.; Romanenko, G.; Ikorskii, V. *Polyhedron* **2005**, *24* (16−17), 2094–2101.

(6) Ovcharenko, V.; Fursova, E.; Romanenko, G.; Eremenko, I.; Tretyakov, E.; Ikorskii, V. *Inorg. Chem.* **2006**, *45*, 5338–5350.

using diamagnetic corrections for the complexes. The effective magnetic moment was calculated as $\mu_{eff} = (8\chi T)^{1/2}$. Experimental temperature dependences of μ_{eff} for all solids were calculated for the {Cu(hfac)$_2$L·0.5Solv} unit. This means that the resulting μ_{eff} value contains two contributions: from $^1/_2$ of >N−•O−Cu^{II}−O•−N< heterospin clusters belonging to the CuO_6 units and from $^1/_2$ of isolated Cu^{II} ions lying in the CuN_2O_4 coordination units. The magnetic data have good reproducibility for different batches of particular complexes. Measurements of $\chi(T)$ were performed at decreasing and increasing temperature for Cu(hfac)$_2$L·0.5C$_6$H$_{14}$ and Cu(hfac)$_2$L·0.5C$_4$H$_9$Br; hysteresis phenomena were not revealed.

Synthesis of Complexes. Cu(hfac)$_2$L: "Head-to-Head" Modification. A mixture of Cu(hfac)$_2$ (0.048 g, 0.10 mmol) and L (0.028 g, 0.10 mmol) was dissolved in acetone (1 mL), and decane (3 mL) was added. The volume of the solution was decreased to ~3 mL with a current of air, and then the solution was kept in an open flask at 5 °C. After 6−8 h, the dark-violet needle crystals were separated by filtration, washed with cold heptane, and dried in air. Yield: 0.041 g, 54%. Anal. Calcd (%) for $C_{24}H_{25}N_4O_6F_{12}Cu$: C, 38.1; H, 3.3; N, 7.4; F, 30.1. Found: C, 38.1; H, 3.6; N, 7.2; F, 29.9. Along with the crystals of the modification formed by the polymer chains with a "head-to-head" motif, we occasionally isolated the crystals of the modification formed by the chains with a "head-to-tail" motif and shaped as elongated prisms. The single crystals of these phases were separated mechanically. If the selected Cu(hfac)$_2$L single crystals of the "head-to-tail" modification were introduced as seed crystals in a saturated hexane solution of the complex, the solid phase was isolated as individual Cu(hfac)$_2$L crystals of the "head-to-tail" modification. Yield: 40−45%. Along with the crystals of the "head-to-tail" modification, Cu(hfac)$_2$L·0.5C$_6$H$_{14}$ crystals could also form in small amounts in the saturated hexane solutions of the complex. The latter crystals differed dramatically from the crystals of the "head-to-tail" modification because they were shaped as rhombohedra and could easily be separated mechanically. If, however, the seed crystals of the "head-to-tail" modification were not introduced in the saturated hexane solutions, the solid phase preferably consisted of "head-to-head" Cu(hfac)$_2$L·0.5C$_6$H$_{14}$ crystals.

α-Cu(hfac)$_2$L·0.5C$_5$H$_{12}$ and β-Cu(hfac)$_2$L·0.5C$_5$H$_{12}$. A mixture of Cu(hfac)$_2$ (0.045 g, 0.094 mmol) and L (0.028 g, 0.10 mmol) was dissolved in *n*-pentane (6 mL). The resulting dark-brown solution was kept in an open flask at room temperature for 8 h. This generally gave a mixture of two types of differently shaped dark-violet crystals, which were filtered off, washed with cold pentane, dried in air, and separated mechanically. The rhombohedral crystals were the polymorphic modification designated below as α-Cu(hfac)$_2$L·0.5C$_5$H$_{12}$, while the elongated prismatic crystals were the polymorphic modification β-Cu(hfac)$_2$L·0.5C$_5$H$_{12}$. Like all other compounds described below, the complexes are well soluble in most organic solvents. **α-Cu(hfac)$_2$L·0.5C$_5$H$_{12}$**. Yield: 20−60%. Anal. Calcd (%) for $C_{27.5}H_{33}N_4O_6F_{12}Cu$: C, 40.1; H, 3.9; N, 7.1; F, 28.8. Found: C, 39.9; H, 3.5; N, 7.2; F, 28.3. **β-Cu(hfac)$_2$L·0.5C$_5$H$_{12}$** Yield: 10−50%. Anal. Calcd (%) for $C_{27.5}H_{33}N_4O_6F_{12}Cu$: C, 40.1; H, 3.9; N, 7.1; F, 28.8. Found: C, 40.2; H, 4.4; N, 6.9; F, 29.3.

Cu(hfac)$_2$L·0.5(C$_2$H$_5$)$_2$O. A mixture of Cu(hfac)$_2$ (0.048 g, 0.10 mmol) and L (0.028 g, 0.10 mmol) was dissolved in Et$_2$O (1 mL), and then decane (3 mL) was added. The resulting dark-brown solution was kept in an open flask at 5 °C for 1 day. The elongated dark-violet crystals were separated by filtration, washed with cold heptane, and dried in air. Yield: 0.045 g, 57%. Anal. Calcd (%) for $C_{52}H_{60}N_8O_{13}F_{24}Cu_2$: C, 39.3; H, 3.8; N, 7.1; F, 28.7. Found: C, 39.6; H, 3.6; N, 7.3; F, 29.5.

Cu(hfac)$_2$L·0.5C$_5$H$_{11}$Cl. A mixture of Cu(hfac)$_2$ (0.048 g, 0.10 mmol) and L (0.028 g, 0.10 mmol) was dissolved in amyl chloride (0.75 mL). The resulting solution was kept in an open small glass jar (5 mL) at room temperature for 1 day. After the solvent evaporated almost completely, dark-violet rhombohedral crystals formed, which were separated by filtration, washed with cold heptane, and dried in air. Yield: 0.033 g, 41%. Anal. Calcd (%) for $C_{26.5}H_{30.5}N_4O_6F_{12}Cl_{0.5}Cu$: C, 39.3; H, 3.8; N, 6.9; F, 28.1; Cl, 2.2. Found: C, 39.5; H, 3.7; N, 6.9; F, 28.1; Cl, 2.2. Cu(hfac)$_2$L·0.5C$_5$H$_{11}$Br, Cu(hfac)$_2$L·0.5C$_5$H$_{11}$I, Cu(hfac)$_2$L·0.5C$_4$H$_9$Cl, and Cu(hfac)$_2$L·0.5C$_4$H$_9$Br were prepared by a similar procedure, in which amyl bromide, amyl iodide, butyl chloride, and butyl bromide, respectively, were used as solvents. **Cu(hfac)$_2$L·0.5C$_5$H$_{11}$Br**. Yield: 0.026 g, 32%. Anal. Calcd (%) for $C_{26.5}H_{30.5}N_4O_6F_{12}Br_{0.5}Cu$: C, 38.2; H, 3.7; N, 6.7; F, 27.4; Br, 4.8. Found: C, 38.5; H, 3.7; N, 6.5; F, 27.3; Br, 4.8. **Cu(hfac)$_2$L·0.5C$_5$H$_{11}$I**. Yield: 0.026 g, 30%. Anal. Calcd (%) for $C_{26.5}H_{30.5}N_4O_6F_{12}I_{0.5}Cu$: C, 37.2; H, 3.6; N, 6.5; F, 26.6; I, 7.4. Found: C, 37.1; H, 3.6; N, 6.9; F, 26.7; I, 7.7. **Cu(hfac)$_2$L·0.5C$_4$H$_9$Cl**. Elongated rhombohedra. Yield: 0.042 g, 52%. Anal. Calcd (%) for $C_{26}H_{29.5}N_4O_6F_{12}Cl_{0.5}Cu$: C, 38.9; H, 3.7; N, 7.0; F, 28.4; Cl, 2.2. Found: C, 39.0; H, 3.7; N, 6.8; F, 28.1; Cl, 2.4. **Cu(hfac)$_2$L·0.5C$_4$H$_9$Br**. Yield: 0.053 g, 64%. Anal. Calcd (%) for $C_{26}H_{29.5}N_4O_6F_{12}Br_{0.5}Cu$: C, 37.8; H, 3.6; N, 6.8; F, 27.6; Br, 4.8. Found: C, 37.6; H, 3.6; N, 7.0; F, 27.2; Br, 4.7. Under similar conditions, synthesis of Cu(hfac)$_2$L·0.5C$_4$H$_9$I gave, in 3 h, large rhombohedral crystals formed at the bottom of the jar. Fine crystals shaped as dark-blue- and claret-colored elongated plates also formed in insignificant amounts on the walls of the vessel. The crystals were separated by filtration, washed with cold heptane, and dried in air. The dark-violet rhombohedra of Cu(hfac)$_2$L·0.5C$_4$H$_9$I, which formed the bulk of the product, were mechanically separated from the impurity of fine plates. Yield: 0.019 g, 22%. Anal. Calcd (%) for $C_{26}H_{29.5}N_4O_6F_{12}I_{0.5}Cu$: C, 36.8; H, 3.5; N, 6.6; F, 26.9; I, 7.5. Found: C, 36.9; H, 3.5; N, 6.6; F, 27.4; I, 7.5.

X-ray Crystallography. The intensity data for the single crystals of the compounds were collected on a SMART APEX CCD (Bruker AXS) automated diffractometer with a Helix (Oxford Cryosystems) open-flow helium cooler using the standard procedure (Mo radiation). The structures were solved by direct methods and refined by a full-matrix least-squares procedure anisotropically for non-hydrogen atoms and isotropically for hydrogen atoms. The hydrogen atoms were located in difference electron density syntheses and calculated geometrically. All calculations were fulfilled with the *SHELXTL 6.14* program package.

Density Functional Theory (DFT) Calculations. All DFT calculations were performed with the *Gaussian 98* program package[7] employing the PBE0 hybrid functional.[8] An accurate all-electron Gaussian basis set of triple-ζ quality with one set of polarization functions Wachters+f = (14s11p6d3f)/[8s6p4d1f][9] was used for the copper atom as obtained from the Extensible

(7) Frisch, M. J.; et al. *Gaussian 98*; Gaussian Inc.: Pittsburgh PA, 1998.
(8) Adamo, C.; Cossi, M.; Barone, V. *J. Mol. Struct. (THEOCHEM)* **1999**, *493*, 145–157.
(9) (a) Wachters, A. J. H. *J. Chem. Phys.* **1970**, *52*, 1033–1036. (b) Wachters, A. J. H. *IBM Tech. Rep.* **1969**, RJ584. (c) Bauschlicher, C. W.; Langhoff, S. R., Jr.; Barnes, L. A. *J. Chem. Phys.* **1989**, *91*, 2399–2411.

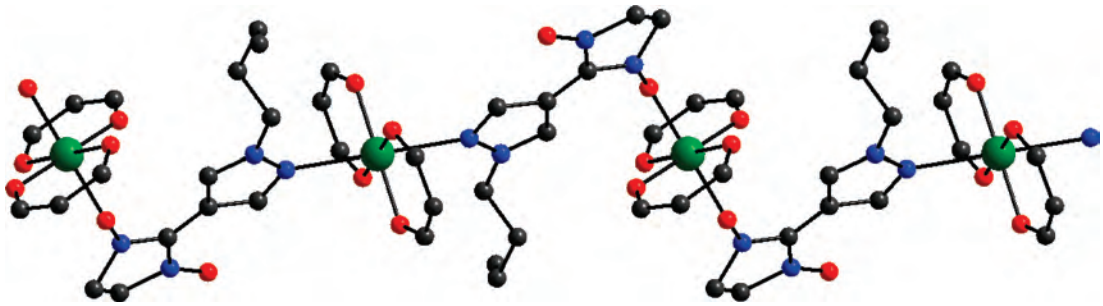

Figure 1. Chain motif in $Cu(hfac)_2L\cdot 0.5C_7H_{16}$. Color code: Cu, green ball; O, red ball; C, black ball; N, blue ball. The hydrogen atoms and the CH_3 and CF_3 groups are omitted for clarity.

Computational Chemistry Environment Basis Set Database.[10] All other atoms (e.g., carbon, nitrogen, oxygen, fluorine, and hydrogen) were described with the polarized 6-31G(d) basis set[11] of double-ζ quality. In all calculations, the exchange-coupled three-spin units L−Cu(hfac)$_2$−L were considered, employing X-ray structural data without further geometry optimization. Theoretical $\mu(T)$ dependences were reconstructed as described elsewhere.[11,12] The molecular orbitals and spin-density distributions were plotted using the *MOLEKEL* program.[13] The broken-symmetry approach[14] was employed to elucidate the magnetic properties of the multispin systems under study. The exchange coupling constants were calculated by the generalized spin projection method suggested by Yamaguchi et al.[15]

Results and Discussion

The discussion of the magnetostructural correlations for the solvates is reasonable to start with a group of compounds $Cu(hfac)_2L\cdot 0.5Solv$, where Solv is hexane, heptane, octane, or octene. We consider a typical example of the structure of a solvate with heptane $Cu(hfac)_2L\cdot 0.5C_7H_{16}$. Figure 1 shows a polymer chain in the solid complex, whose general motif is identical with the polymer chains in all other compounds discussed below. In the chains constructed based on the "head-to-head" motif, the Cu^{II} ions lying in the CuN_2O_4 coordination units alternate with the >N−•O−Cu^{II}−O•−N< heterospin clusters belonging to the CuO_6 units. Thus, the CuO_4 square environment in the $Cu(hfac)_2$ coordination matrices is completed to a distorted octahedron either by two nitrogen atoms of the pyrazole rings of the two bridging bidentate L or by two oxygen atoms of the nitronyl nitroxide fragments. The second oxygen atom of the nitronyl nitroxide fragment is not involved in coordination. The structure dynamics of the chains due to variation of the temperature are mainly related to the rearrangement of the CuN_2O_4 and CuO_6 coordination units.

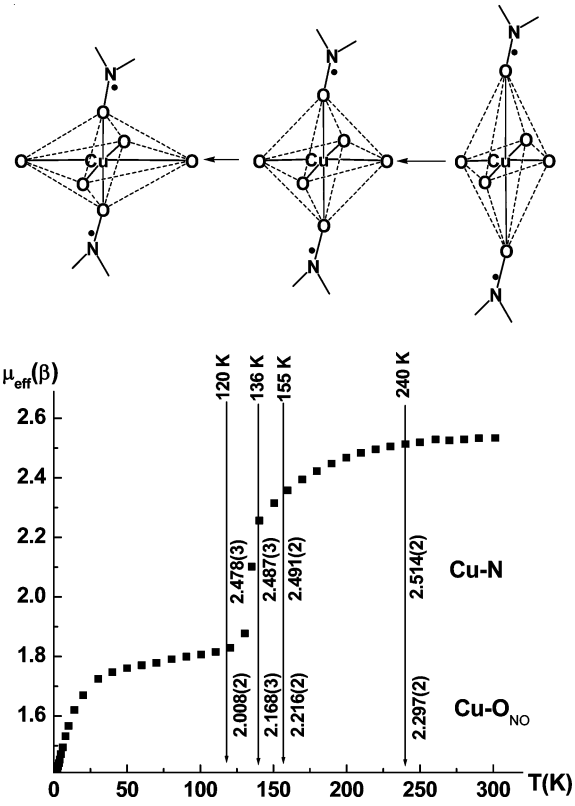

Figure 2. Temperature dependence of the effective magnetic moment of $Cu(hfac)_2L\cdot 0.5C_7H_{16}$ (■). The vertical arrows indicate the temperature of the X-ray diffraction experiment; the upper and lower lines of the figures correspond to the Cu−N and Cu−O_{NO} bond lengths in the CuN_2O_4 and CuO_6 units, respectively.

Figure 2 shows the experimental temperature dependence of μ_{eff} for $Cu(hfac)_2L\cdot 0.5C_7H_{16}$, where the vertical arrows indicate the temperatures at which the crystal and molecular structures were determined for the single crystal of the complex. Full structural data are presented in the Supporting Information. In Figure 2, only the Cu−N bond lengths in the CuN_2O_4 units (the upper line of figures) and the Cu−O_{NO} bond lengths in the CuO_6 units (the lower line) at the

(10) Basis sets were obtained from the Extensible Computational Chemistry Environment Basis Set Database, Version 02/02/06, as developed and distributed by the Molecular Science Computing Facility, Environmental and Molecular Sciences Laboratory, which is part of the Pacific Northwest Laboratory, P.O. Box 999, Richland, WA 99352, and funded by the U.S. Department of Energy. The Pacific Northwest Laboratory is a multi-program laboratory operated by Battelle Memorial Institute for the U.S. Department of Energy under Contract DE-AC06-76RLO 1830. Contact Karen Schuchardt for further information.

(11) Davidson, E. R.; Feller, D. *Chem. Rev.* **1986**, *86*, 681–696.

(12) Gorelik, E. V.; Ovcharenko, V. I.; Baumgarten, M. *Eur. J. Inorg. Chem.* **2008**, 2837–2846.

(13) Flükiger, P.; Lüthi, H. P.; Portmann, S.; Weber, J. *MOLEKEL 4.0*; Swiss National Supercomputing Centre CSCS: Manno, Switzerland, 2000.

(14) (a) Daul, C. A.; Ciofini, I.; Bencini, A. In *Reviews of Modern Quantum Chemistry*; Sen, K. D., Ed.; World Scientific: Singapore, 2002; Part II, p 1247. (b) Noodleman, L.; Peng, C. Y.; Case, D. A.; Mouesca, J. M. *Coord. Chem. Rev.* **1995**, *144*, 199. (c) Noodleman, L.; Norman, J. G., Jr *J. Chem. Phys.* **1979**, *70*, 4903.

(15) (a) Shoji, M.; Koizumi, K.; Kitagawa, Y.; Kawakami, T.; Yamanaka, S.; Okumura, M.; Yamaguchi, K. *Chem. Phys. Lett.* **2006**, *432*, 343. (b) Soda, T.; Kitagawa, Y.; Onishi, T.; Takano, Y.; Shigeta, Y.; Nagao, H.; Yoshioka, Y.; Yamaguchi, K. *Chem. Phys. Lett.* **2000**, *319*, 223. (c) Yamaguchi, K.; Jensen, F.; Dorigo, A.; Houk, K. N. *Chem. Phys. Lett.* **1988**, *149*, 537.

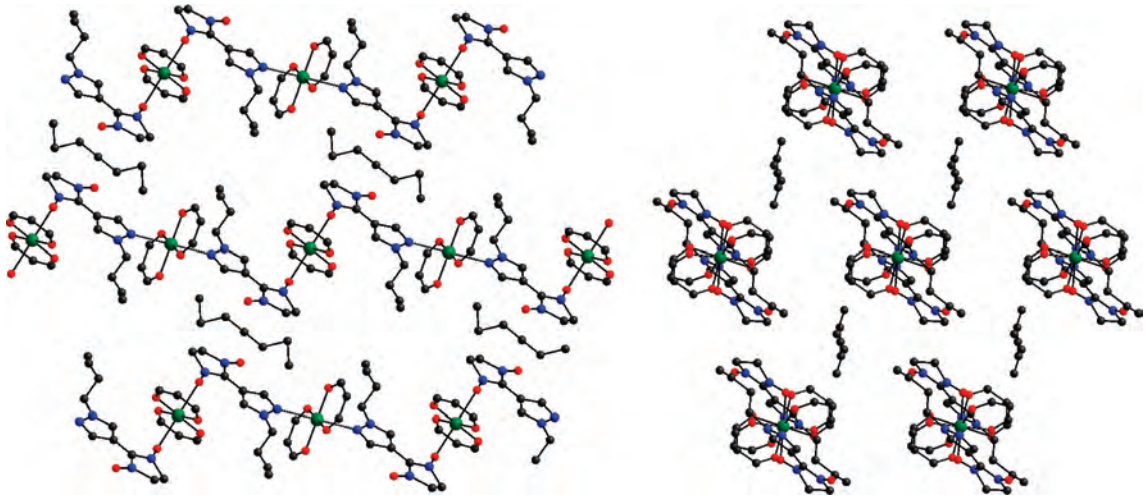

Figure 3. Packing of $Cu(hfac)_2L\cdot 0.5C_7H_{16}$ in the high-temperature phases. Left: view along one of the directions perpendicular to the chains. Right: view along the chains.

corresponding temperature are given to avoid encumbering with many structural parameters. These data show that, with a decrease in the temperature, the $Cu-O_{NO}$ bond lengths in the CuO_6 units are drastically reduced. This shortening of the $Cu-O_{NO}$ bonds is accompanied by simultaneous lengthening of two $Cu-O_{hfac}$ bonds from 1.988(2) to 2.280(2) Å in one of the directions when the crystal is cooled from 240 to 120 K; i.e., with a decrease in the temperature, the direction change of the elongated Jahn−Teller axis takes place in the CuO_6 units. At high temperatures, this is the $O_{NO}-Cu-O_{NO}$ axis, while at low temperatures, it is the $O_{hfac}-Cu-O_{hfac}$ axis (the upper part of Figure 2). According to X-ray diffraction data, at ∼135 K the coordination polyhedra of the CuO_6 units take the form of a flattened octahedron, which is rarely met in Cu^{II} compounds. The value of μ_{eff}, which decreased gradually in the range 300−140 K, decreases sharply at 135 K. As a result, the magnetic moment, which was equal to 2.52 μ_B at room temperature, becomes 1.78 μ_B in the range 30−100 K, which corresponds to its decrease by a factor of $\sqrt{2}$ or to a decrease by a factor of 2 in the total number of spins. Following[1] from this, we can also conclude that, in all $>N-^{\bullet}O-Cu^{II}-O^{\bullet}-N<$ exchange clusters, a very strong antiferromagnetic exchange interaction dominates below 135 K, which is just responsible for the vanishing contribution to magnetic susceptibility from half of the total number of spins. In the CuN_2O_4 units, the Cu−N distances are also shortened at reduced temperatures but to a smaller extent than the $Cu-O_{NO}$ distances (Figure 2).

It is worth noting that, in all solid solvates, the packing mode of polymer chains is the same (in Figure 3, this packing is shown for $Cu(hfac)_2L\cdot 0.5C_7H_{16}$; in Figure 3SI (Supporting Information) is shown the similarity of packings of the $Cu(hfac)_2L\cdot 0.5C_6H_{14}$, $Cu(hfac)_2L\cdot 0.5C_7H_{16}$, $Cu(hfac)_2L\cdot 0.5C_8H_{18}$, and $Cu(hfac)_2L\cdot 0.5C_8H_{16}$ solvates). The regions with solvate molecules are also identical. The only difference is the volume occupied by the solvent molecules and the character of twisting of hydrocarbon chains inside the cavities that they occupy.

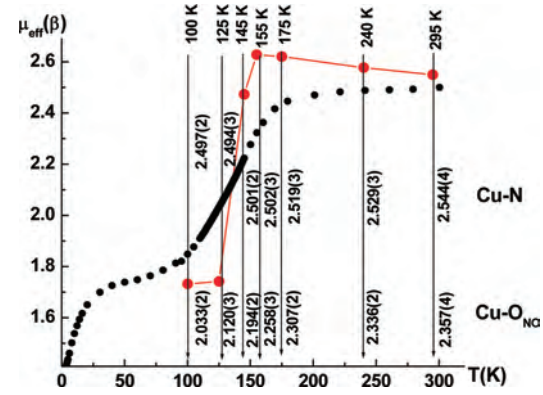

Figure 4. Temperature dependence of the effective magnetic moment of $Cu(hfac)_2L\cdot 0.5C_8H_{18}$ (●). The vertical arrows indicate the temperature of the X-ray diffraction experiment; the upper and lower lines of the figures correspond to the Cu−N and $Cu-O_{NO}$ bond lengths in the CuN_2O_4 and CuO_6 units, respectively. The values obtained by quantum-chemical calculations are shown by the filled red circles and connected by the red lines to demonstrate a good agreement between the experimental and calculated $\mu_{eff}(T)$ dependences.

For solvates with octane and octene molecules, the structural rearrangement of the CuO_6 and CuN_2O_4 coordination polyhedra during the phase transition is similar to the structural rearrangements in $Cu(hfac)_2L\cdot 0.5C_7H_{16}$. With a decrease in the temperature, the $Cu-O_{NO}$ distances in the above solvates are considerably shortened, from 2.336(2) Å (240 K) to 2.033(2) Å (100 K) in $Cu(hfac)_2L\cdot 0.5C_8H_{18}$ and from 2.331(2) Å (240 K) to 1.995(2) Å (100 K) in $Cu(hfac)_2L\cdot 0.5C_8H_{16}$. The $Cu-O_{NO}$ and Cu−N bond lengths at other temperatures are shown in Figures 4 and 5. The shortening of the $Cu-O_{NO}$ distances is accompanied by a change of the axial direction of the Jahn−Teller axis in the CuO_6 coordination units from $O_{NO}-Cu-O_{NO}$ to $O_{hfac}-Cu-O_{hfac}$. As in the case of the heptane solvate, the Cu−N distances in the CuN_2O_4 coordination units are shortened to a much smaller extent [from 2.529(3) Å (240 K) to 2.497(2) Å (100 K) in $Cu(hfac)_2L\cdot 0.5C_8H_{18}$ and from 2.524(2) Å (240 K) to 2.461(3) Å (100 K) in $Cu(hfac)_2L\cdot 0.5C_8H_{16}$; Figures 4 and 5, respectively].

Because the changes in the bond lengths in the $>N-^{\bullet}O-Cu^{II}-O^{\bullet}-N<$ exchange clusters during the low-

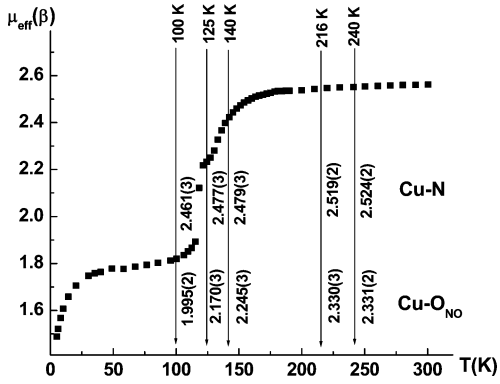

Figure 5. Temperature dependence of the effective magnetic moment of $Cu(hfac)_2L\cdot 0.5C_8H_{16}$ (■). The vertical arrows indicate the temperature of the X-ray diffraction experiment; the upper and lower lines of the figures correspond to the Cu−N and $Cu-O_{NO}$ bond lengths in the CuN_2O_4 and CuO_6 units, respectively.

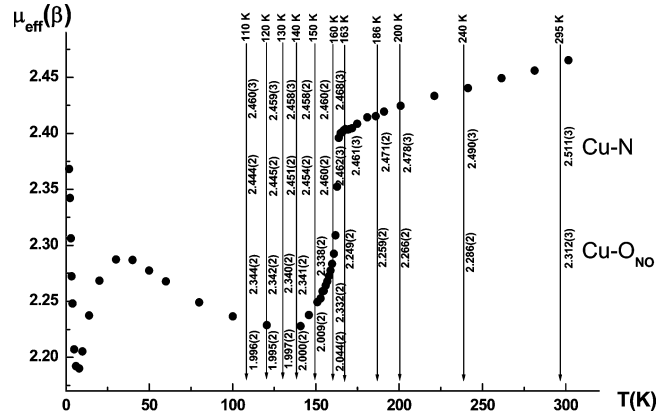

Figure 6. Temperature dependence of the effective magnetic moment of $Cu(hfac)_2L\cdot 0.5C_6H_{14}$ (●). The vertical arrows indicate the temperature of the X-ray diffraction experiment; the upper and lower lines of the figures correspond to the Cu−N and $Cu-O_{NO}$ bond lengths in the CuN_2O_4 and CuO_6 units, respectively.

temperature phase transition in $Cu(hfac)_2L\cdot 0.5C_8H_{18}$ and $Cu(hfac)_2L\cdot 0.5C_8H_{16}$ are similar to the changes in $Cu(hfac)_2L\cdot 0.5C_7H_{16}$, one can expect that the magnetic anomalies on the $\mu_{eff}(T)$ curves for $Cu(hfac)_2L\cdot 0.5C_8H_{18}$ and $Cu(hfac)_2L\cdot 0.5C_8H_{16}$ will be similar to the magnetic anomaly for $Cu(hfac)_2L\cdot 0.5C_7H_{16}$ (Figures 2, 4, and 5). In the low-temperature region, μ_{eff} decreased by a factor of $\sqrt{2}$ because of the strong antiferromagnetic exchange interactions in the >N−•O−Cu^{II}−O•−N< exchange clusters, eliminating the contribution of half of all spins to the magnetic susceptibility. Note that, for solvates with heptane and octene, μ_{eff} at first decreases gradually upon cooling and then abruptly at 135 and 118 K for $Cu(hfac)_2L\cdot 0.5C_7H_{16}$ and $Cu(hfac)_2L\cdot 0.5C_8H_{16}$, respectively. The magnetic anomaly for $Cu(hfac)_2L\cdot 0.5C_8H_{16}$ in general seems to be a two-step anomaly. However, analysis of X-ray diffraction data did not reveal any specific structural changes in the range 100−140 K corresponding to the change in the ground state of the >N−•O−Cu^{II}−O•−N< exchange clusters in the CuO_6 units. Therefore, we cannot yet say unambiguously whether this is a two-step anomaly or a kinetic peculiarity of the induction period, at which seeds of the low-temperature phase are accumulated against the background of exchange interactions with the positive sign in the >N−•O−Cu^{II}−O•−N< clusters.

For the solvate with octane, the $\mu_{eff}(T)$ curve does not show any abrupt changes. The transition from the high- to low-spin state upon cooling occurs smoothly within a wide temperature range, 175−75 K. This feature will be discussed after the magnetostructural correlations for the hexane solvate.

Structural analysis of the $Cu(hfac)_2L\cdot 0.5C_6H_{14}$ hexane solvate at 11 temperatures (Figure 6) showed that transformation of the coordination polyhedra in this compound differed significantly from the transformations discussed above. At room temperature, all CuO_6 units are elongated octahedra with axial distances $Cu-O_{NO}$ 2.313(3) Å and equatorial distances $Cu-O_{hfac}$ 1.972(2) and 1.983(2) Å. The CuN_2O_4 units are also octahedra, in which the Cu−N axial distances are rather long [2.511(3) Å], while the $Cu-O_{hfac}$ equatorial distances are much shorter, 1.940(2) and 1.973(3) Å. According to X-ray data, when the temperature is lowered to 163 K, the $Cu-O_{NO}$ distances in the CuO_6 coordination units are gradually shortened from 2.313(3) to 2.249(2) Å. At still lower temperatures (160 K), the independent part of the structure and hence the cell volume are doubled. The CuN_2O_4 units in $Cu(hfac)_2L\cdot 0.5C_6H_{14}$ become pseudocentrosymmetric and have different Cu−N distances, 2.462(3) and 2.468(3) Å. The CuO_6 units, however, remain centrosymmetric but are divided into two types. In units of the first type, the axial $Cu-O_{NO}$ distances are lengthened [2.249(2) → 2.332(2) Å]. In units of the second type, the $Cu-O_{NO}$ distances are drastically shortened [2.249(2) → 2.044(2) Å], the O_{NO} atoms in these units pass to the equatorial positions, and two O_{hfac} atoms are ousted to the axial positions [2.021(2) → 2.179(3) Å]. As a result, a structural phase transition occurs in $Cu(hfac)_2L\cdot 0.5C_6H_{14}$ at 161 ± 3 K, and the $Cu-O_{NO}$ distances are shortened in half of all >N−•O−Cu^{II}−O•−N< exchange clusters. This gives rise to a strong antiferromagnetic interaction in these clusters. The effective spin of these triads decreases to $^1/_2$, and the magnetic moment drastically decreases in the range 161 ± 3 K. In the other half of the >N−•O−Cu^{II}−O•−N< exchange clusters, the $Cu-O_{NO}$ distances increase, which favors the ferromagnetic exchange interactions;[1b] therefore, after the region of the structural transition, μ_{eff} ceases to decrease and starts to gradually increase at T < 150 K (Figure 6). Thus, the observed character of $\mu_{eff}(T)$ for $Cu(hfac)_2L\cdot 0.5C_6H_{14}$ completely correlates with the structure dynamics of the heterospin complexes from high to low temperatures.

In discussing the character of the $\mu_{eff}(T)$ dependence for $Cu(hfac)_2L\cdot 0.5C_6H_{14}$, we emphasize that this work focuses on the thermally induced significant structural changes inside the >N−•O−Cu^{II}−O•−N< exchange clusters. Their structural rearrangement leads to a considerable change in the intracluster exchange interaction, which just shows itself as an anomaly on the $\mu_{eff}(T)$ curve. The far weaker intercluster and interchain magnetic interactions at lower temperatures (<50 K) were not analyzed. We only note that, for the majority of the compounds being discussed, the dominant interactions below 50 K are the antiferromagnetic exchange interactions. The appreciable contributions from the ferromagnetic exchange interactions show themselves as the

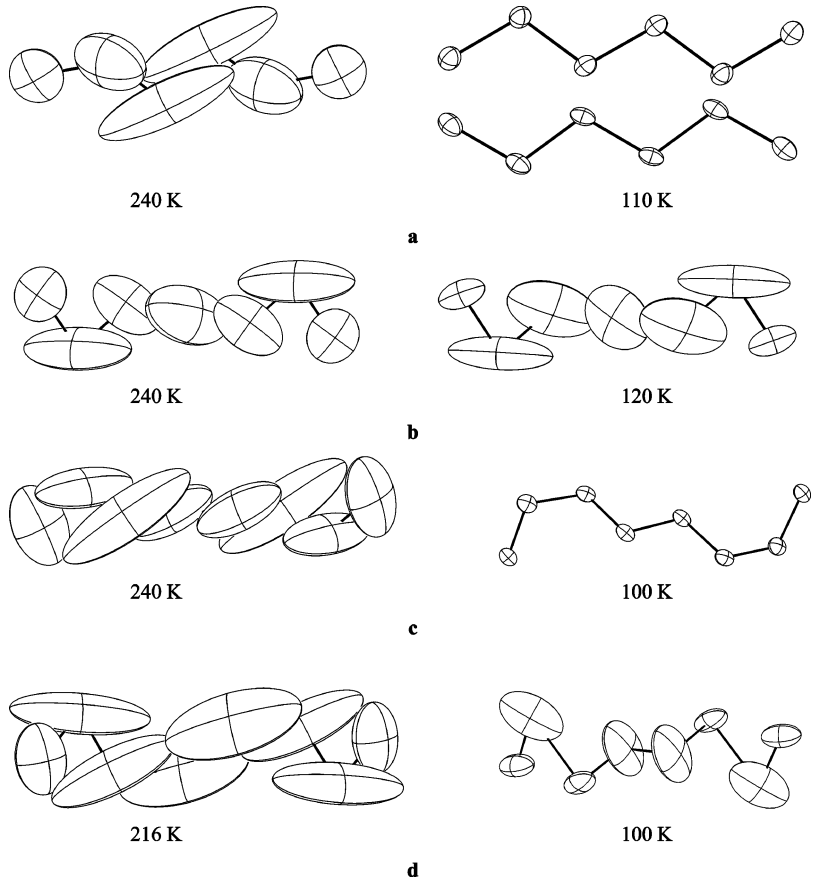

Figure 7. Variation of the thermal ellipsoids of the carbon atoms of the solvent molecules upon passing from the high- to low-temperature phase for $Cu(hfac)_2L\cdot 0.5C_6H_{14}$ (a), $Cu(hfac)_2L\cdot 0.5C_7H_{16}$ (b), $Cu(hfac)_2L\cdot 0.5C_8H_{18}$ (c), and $Cu(hfac)_2L\cdot 0.5C_8H_{16}$ (d). The ellipsoids are drawn at 35% probability.

increased effective magnetic moment at low temperatures for $Cu(hfac)_2L\cdot 0.5C_6H_{14}$ and also for β-$Cu(hfac)_2L\cdot 0.5C_5H_{12}$, $Cu(hfac)_2L$, $Cu(hfac)_2L\cdot 0.5C_5H_{11}Br$, and $Cu(hfac)_2L\cdot 0.5C_5H_{11}Cl$ discussed below. As shown elsewhere,[12] a special investigation is needed in order to explain their formation.

Although the temperature range of the magnetic anomaly for $Cu(hfac)_2L\cdot 0.5Solv$ (Solv = C_6H_{14}, C_7H_{16}, C_8H_{18}, and C_8H_{16}) in general is rather narrow, from 118 to 161 K, the shape of the anomaly is the same only for $Cu(hfac)_2L\cdot 0.5C_7H_{16}$ and $Cu(hfac)_2L\cdot 0.5C_8H_{16}$ (Figures 2 and 5). For $Cu(hfac)_2L\cdot 0.5C_8H_{18}$ (Figure 4) and especially $Cu(hfac)_2L\cdot 0.5C_6H_{14}$ (Figure 6), it is substantially different. It was very difficult to predict this difference in the structural rearrangements of the solids and hence in the magnetic behavior of solvates with very similar packings (Figure 3 and Figure 3SI in the Supporting Information). The fact that the change in the number of methylene units in the uncoordinated molecules of organic solvents not linked by hydrogen bonds can lead to substantial changes in the form of $\mu_{eff}(T)$ points to a significant contribution of the interchain interactions and a high degree of cooperativity of this phenomenon. Note that, in solid solvates, there are many contacts between the polymer chains and the solvent molecules, as well as between the adjacent polymer chains; from all of these contacts, *it is very difficult to figure out the most important ones*, especially because the set of these contacts changes in the course of the structural rearrangement of the solid phase. However, one can trace several features that characterize these structural transformations.

If we use the temperature coordinate along with the spatial ones, that is, if we pass to the four-dimensional space, we can reconstruct the structure dynamics in general. These X-ray movies are given for $Cu(hfac)_2L\cdot 0.5C_6H_{14}$ and the solvate cavities of $Cu(hfac)_2L\cdot 0.5C_6H_{14}$ and $Cu(hfac)_2L\cdot 0.5C_7H_{16}$ in the Supporting Information. They provide visualization of the structural rearrangement in the additional coordinate of temperature and actually justify the validity of the term "breathing crystals".

It is also useful to consider changes in the thermal ellipsoids of the carbon atoms of the solvent molecules upon passing from the high- to low-temperature phase (Figure 7). It can be seen that above 200 K the solid solvates have enough space for disordering of the carbon atoms.

The smallest ellipsoids are characteristic of the terminal carbon atoms, which rest against the polymer chains. This is illustrated by Figure 8, which gives an example of contacts between the hexane molecule and the neighboring CF_3 groups of the polymer chains. With a decrease of the temperature, the crystals are compressed, and their density increases. The compression is also accompanied by a decrease in the size of the cavities accommodating the solvate molecules (Table 1; see lines for C_6H_{14}, C_7H_{16}, C_8H_{16}, and C_8H_{18}). It seems that because of the size of the hexane molecules in $Cu(hfac)_2L\cdot 0.5C_6H_{14}$, which are the smallest in the series under study, in the low-temperature phase, the distances are shortened in

Table 1. Characteristics of Magnetic Anomalies for $Cu(hfac)_2L\cdot 0.5Solv$: T_a, Abruptness, the Fraction of Odd Spins Paired during Phase Transition (N), and the Volume of the Cavity Occupied by the Solvent Molecule below (≤120 K) and above (240 K) the Transition

				V_{Solv}, Å^3	
Solv	T_a, K	abruptness	N	≤120 K	240 K
C_7H_{16}	135 ± 3	abrupt	1/2	264	289
C_8H_{18}	~130	gradual	1/2	274	319
C_8H_{16}	118 ± 3	abrupt	1/2	240	330
C_6H_{14}	161 ± 3	abrupt	1/4[a]	253; 254[a]	269
C_5H_{12} (α)	160 ± 3	abrupt	1/2	239	239
C_5H_{12} (β)				169	166
Et_2O				123	166
no solvent	75 ± 3	abrupt	1/4		
$C_5H_{11}Cl$	155 ± 3	abrupt	1/4[a]	233; 250[a]	271
$C_5H_{11}Br$	150 ± 3	abrupt	1/4[a]	247; 260[a]	270
$C_5H_{11}I$	197 ± 4	abrupt	increasing μ_{eff}	272	288
C_4H_9Cl	107 ± 3	abrupt	increasing μ_{eff}	219 (230[b])	224
C_4H_9Br	133 ± 1	abrupt	1/2	238	264
C_4H_9I	160 ± 3	abrupt	1/2	232	262

[a] The independent part of the structure and the unit cell volume are doubled during the transition of the high-temperature polymorph to the low-temperature one. [b] At 30 K.

only half of all CuO_6 units, and the phase transition occurs at 161 ± 3 K. In this case, however, the hexane molecules completely lose their ability to disorder (Figure 7a).

For the solvate with heptane molecules (Figure 7b), which are larger, the transition demands compression of all CuO_6 units and a lower temperature (135 ± 3 K). Although the thermal ellipsoids of the terminal methyl groups decrease considerably after the transition, the carbon atoms of the methylene units retain certain mobility. As the number of methylene units increases further upon passing to the solvate with octane, the solvate molecule is enlarged further and demands lower temperatures (129 ± 3 K) for a transition. Because the octane molecules are larger, they cannot be involved in spatial vibrations, with their thermal ellipsoids becoming small. Note that the octane molecules possess the largest number of C−C single bonds in the series and are therefore favorable for the largest number of various conformations (are the "softest"). It is quite possible that this circumstance is just responsible for the smoothness of the spin transition in $Cu(hfac)_2L\cdot 0.5C_8H_{18}$ (Figure 4). Therefore, in this case, the transition temperature T_a was determined from X-ray diffraction data (see Figure 4SI in the Supporting Information) but not from the maximum point of the $\mu_{eff}(T)$ derivative.

The octene molecules are slightly smaller than the octane ones. However, because of the structural rigidity of the $H_2C{=}CHC$ terminal fragment, the transition demands greater compression, that is, cooling of the compound to a lower temperature (118 ± 3 K).

While the interchain hydrocarbons possess enough freedom for spatial motions, the ability to undergo disordering in the polymer chains is inherent only in the fluorine atoms of the CF_3 groups of the bischelate fragments and the terminal butyl groups, for which changes in orientation due to temperature variation can be visualized with the aid of X-ray movies (in the Supporting Information). However, the structure of the paramagnetic ligand itself remains rigid. Thus, the distances between the coordinated nitrogen atoms of the pyrazole ring and the oxygen atoms of the nitronyl nitroxide fragment in each L change only slightly because of temperature or solvent variation. For example, in $Cu(hfac)_2L\cdot 0.5C_6H_{14}$, this distance changes from 4.962(4) Å at 295 K to 4.974(3) and 4.966(4) Å at 110 K. The angle between the planes of the pyrazole ring and the CN_2 fragment of the imidazoline ring also changes insignificantly, from ~2.5(2) to 3.6(3)°. These data confirm that main structural transformations in the polymer chains are caused by the considerable changes in the $Cu{-}O_{NO}$, $Cu{-}O_{hfac}$, and Cu−N distances in the CuO_6 and CuN_2O_4 coordination units.

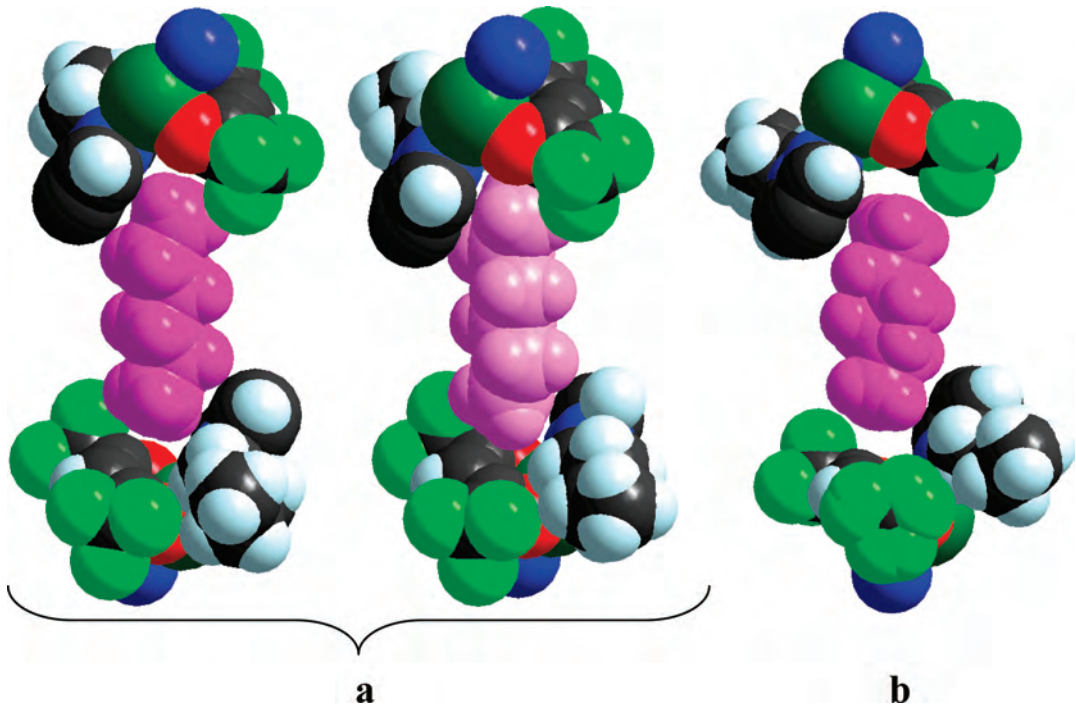

Figure 8. Environment of the hexane molecules in $Cu(hfac)_2L\cdot 0.5C_6H_{14}$ at 110 K (a) and 295 K (b).

In the examples discussed above, the greatest changes occurred in the CuO_6 units, which were responsible for the magnetic anomaly. However, a situation is possible when changes in the structure are mostly determined by changes in the Cu−N bond lengths. We encountered this situation when investigating the polymorphic modifications of the pentane and diethyl ether solvates. Two polymorphic modifications, α-Cu(hfac)$_2$L·0.5C_5H_{12} and β-Cu(hfac)$_2$L·0.5C_5H_{12}, were isolated as solids from pentane; they differed in the mutual arrangement of chains and arrangement of solvent molecules between them. Parts a and b of Figure 9 show the chain packings in the α-Cu(hfac)$_2$L·0.5C_5H_{12} and β-Cu(hfac)$_2$L·0.5C_5H_{12} polymorphic modifications. In the left parts of parts a and b of Figure 9, the projection orthogonal to the chains indicates that the pentane molecules are differently oriented relative to the chains. The right parts of parts a and b of Figure 9 show projections along the chains, and the difference in the arrangement of solvate molecules is even larger. Figure 9SI in the Supporting Information gives analogous projections for the diethyl ether solvate, Cu(hfac)$_2$L·0.5Et_2O. This solvate is discussed here because its pentaatomic molecules are topologically identical with the pentane molecules. In the course of synthesis, it was isolated as a single modification, whose structure proved fully identical with that of β-Cu(hfac)$_2$L·0.5C_5H_{12}.

The packing of chains and solvate molecules in α-Cu(hfac)$_2$L·0.5C_5H_{12} are the same (Figure 9a) as those in solvates with other saturated hydrocarbon solvents (Figure 3). It is not surprising, therefore, that the $\mu_{eff}(T)$ dependence, as well as the character of variation of the Cu−N and Cu−O_{NO} bond lengths for α-Cu(hfac)$_2$L·0.5C_5H_{12} (Figure 10), are similar to those for Cu(hfac)$_2$L·0.5C_7H_{16} (Figure 2). For β-Cu(hfac)$_2$L·0.5C_5H_{12} and Cu(hfac)$_2$L·0.5Et_2O, the Cu−O_{NO} distances are the largest among the solvates and change only insignificantly with a decrease in the temperature (Figure 11), while the Cu−N distances decrease considerably. Because the CuO_6 units, involving the >N−•O−Cu^{II}−O•−N< exchange clusters, do not undergo any pronounced changes in structure, the $\mu_{eff}(T)$ curve for these compounds does not show any magnetic anomalies (Figure 11). Thus, the different mode of packing for solvent molecules in the interchain space in solid β-Cu(hfac)$_2$L·0.5C_5H_{12} and Cu(hfac)$_2$L·0.5Et_2O led to a different structural transformation of the coordination units of the polymer chains, which involved mainly the CuN_2O_4 units and thus precluded the magnetic anomalies. The experimental $\mu_{eff}(T)$ dependence for both β-Cu(hfac)$_2$L·0.5C_5H_{12} and Cu(hfac)$_2$L·0.5Et_2O can be fitted uniformly over the whole temperature range. This is well described by the following set of optimum parameters: for Cu(hfac)$_2$L·0.5Et_2O, $g_{Cu} = 2.18(2)$, $J = 11.8(6)$ cm^{-1}, $nJ' = -0.8(1)$ cm^{-1}; for β-Cu(hfac)$_2$L·0.5C_5H_{12}, $g_{Cu} = 2.39(1)$, $J = 13.6(5)$ cm^{-1}, $nJ' = -0.063(6)$ cm^{-1}; g_L was set as 2.00. The experimental data were described using the isotropic spin Hamiltonian $\hat{H} = -2J\hat{s}_{Cu}\hat{s}' - (2g_{Cu}\hat{s}_{Cu} + g_{NO}\hat{s}')\beta H - 2nJ'\hat{S}\langle S\rangle$, in which $s' = s_{NO1} + s_{NO2}$ is the total spin of two coordinated >N−•O groups in the exchange cluster, $S = 2s_{Cu} + s'$ is the total spin of the complex, J is the intracluster exchange parameter, and nJ' is the intercluster exchange parameter.[16]

It is worth noting that Cu(hfac)$_2$L·0.5C_7H_{16} is the most kinetically stable solvate, being stable even in a vacuum chamber. Octane and octene solvates are less stable and slowly decompose at ambient conditions within 2−3 days. Moreover, Cu(hfac)$_2$L cannot include solvate molecules larger than octane. Crystallization from nonane and decane gave only solid Cu(hfac)$_2$L. The packing of polymer chains in this compound has certain distinctions from the packing in the solvates (Figure 9c). For Cu(hfac)$_2$L, the magnetic anomaly shows itself at quite a low temperature, 75 ± 3 K (Figure 12), and the Cu−O_{NO} distances are drastically shortened in only half of all CuO_6 coordination units.

The search for analogies between the magnetic properties of Cu(hfac)$_2$L·0.5Solv, where Solv is C_5H_{12} (α modification), C_7H_{16}, C_8H_{18}, and C_8H_{16}, and the magnetic properties of β-Cu(hfac)$_2$L·0.5C_5H_{12}, Cu(hfac)$_2$L·0.5Et_2O, and especially Cu(hfac)$_2$L is hindered by the fact that for the latter three compounds the packing of chains changes significantly. However, as shown by our study, within the isostructural series of pentane, hexane, heptane, and octane solvates, *the homologous step of one methylene unit intrinsic in organic chemistry proved too large in the amount of its action on the magnetic effect under discussion*. If the experimental $\mu_{eff}(T)$ curves for solvates with a similar structure involving pentane (Figure 10), hexane (Figure 6), heptane (Figure 2), and octane (Figure 4) are superimposed on one another, it will be clear that the amplitude and character of the magnetic anomaly are different.

This prompted us to adopt a smaller step in structure variation of the incorporated solvent molecule. For this, we used amyl chloride, bromide, and iodide as the spatial analogues of hexane, whose Cu(hfac)$_2$L·0.5C_6H_{14} solvate had the most sophisticated $\mu_{eff}(T)$ dependence. Below we give a reference scale, which depicts the difference in the radii of the terminal groups or atoms attached to the amyl fragment and is constructed from reference data on the covalent atomic radii (Chart 1).[17] If we adopt the methyl group as a reference point, its substitution by a chlorine atom leads to a certain decrease in the size of the terminal fragment. Replacement of the methyl group by a bromine atom, however, will lead to a minor increase in the size of the terminal fragment. Substitution of the methyl group by an iodine atom will cause a substantial increase in the linear dimension of the terminal group. The largest increase on the scale is caused by the substitution of the methyl by an ethyl group. In the latter case, it was adopted that the ethyl fragment was bonded to the amyl fragment at an angle of 109°. The packing of chains is the same in the hexane and heptane, as well as in amyl chloride, bromide, and iodide solvates. The same relates to the motif of the

(16) (a) Tretyakov, E.; Fokin, S.; Romanenko, G.; Ikorskii, V.; Vasilevsky, S.; Ovcharenko, V. *Inorg. Chem.* **2006**, *45*, 3671–3678. Ovcharenko, I. V.; Shvedenkov, Yu. G.; Musin, R. N.; Ikorskii, V. N. *Russ. J. Struct. Chem.* **1999**, *40*, 29–34.

(17) Gordon, A. J.; Ford, R. A. *The Chemist's Companion. A Handbook of Practical Data, Techniques, and References*; John Wiley and Sons: New York, 1972; pp 95−101.

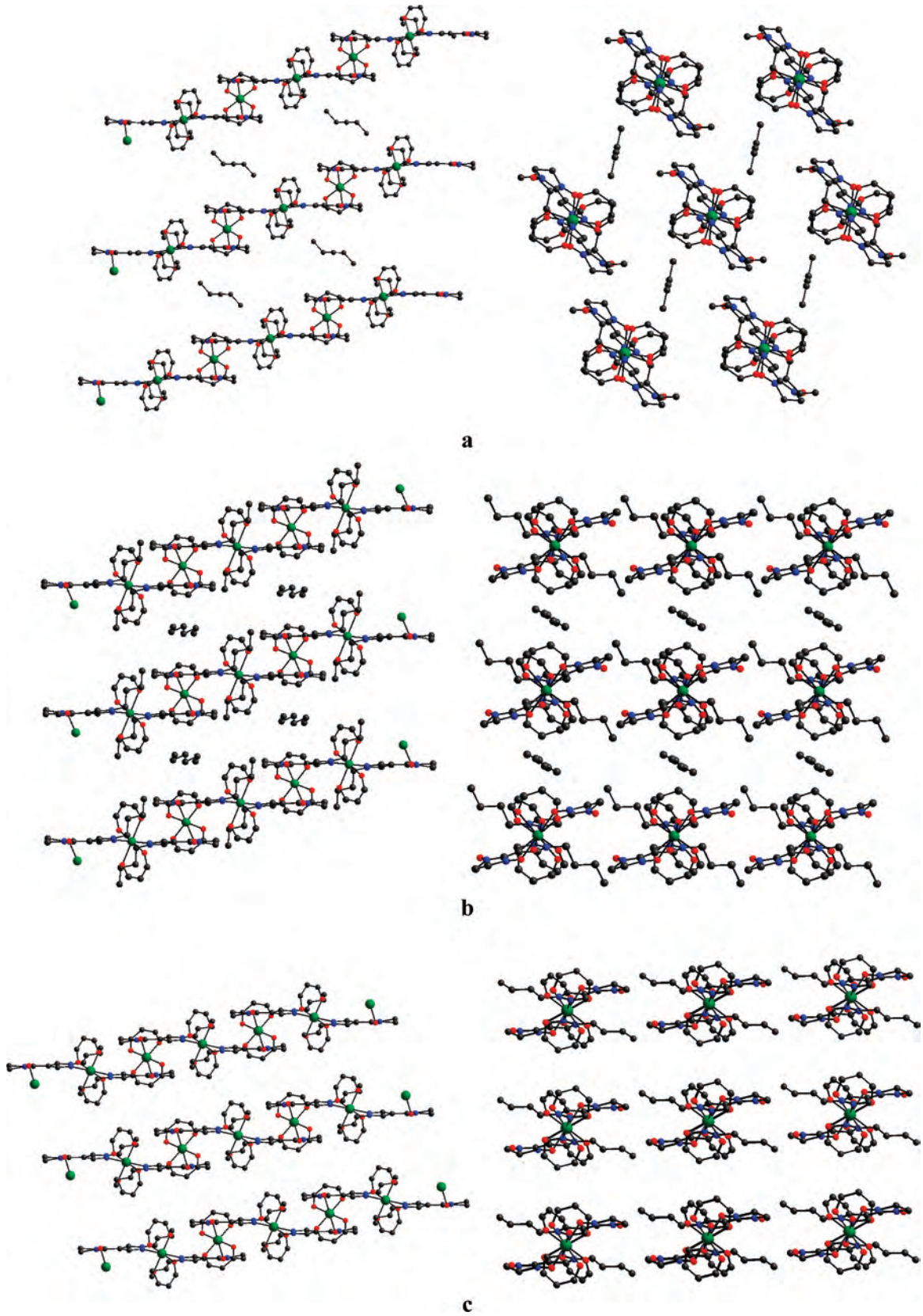

Figure 9. Packing of chains in α-$Cu(hfac)_2L \cdot 0.5C_5H_{12}$ (a), β-$Cu(hfac)_2L \cdot 0.5C_5H_{12}$ (b), and $Cu(hfac)_2L$ (c).

arrangement of the solvate molecules (Figure 3), whose terminal fragments rest against the rosettes of the CF_3 groups of the hexafluoroacetylacetonate fragments (Figure 8). If the electronic and polarization effects make only a small contribution, one could expect the amyl bromide and chloride solvates to be closest to $Cu(hfac)_2L \cdot 0.5C_6H_{14}$ in structure dynamics and hence in the magnetic behavior.

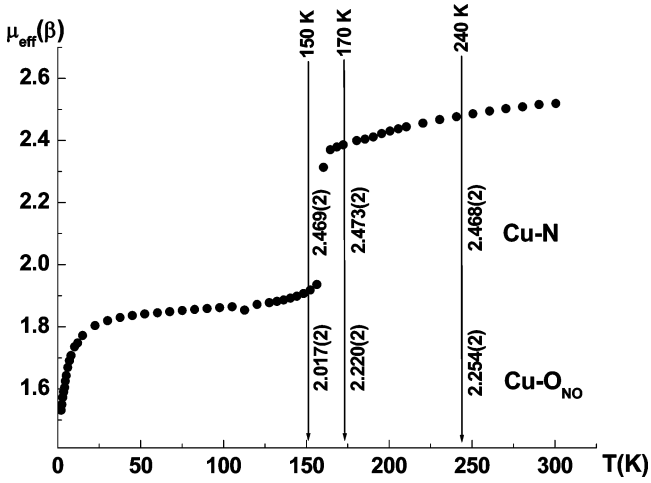

Figure 10. Temperature dependence of the effective magnetic moment of α-Cu(hfac)$_2$L·0.5C$_5$H$_{12}$ (●). The vertical arrows indicate the temperature of the X-ray diffraction experiment; the upper and lower lines of the figures correspond to the Cu−N and Cu−O$_{NO}$ bond lengths in the CuN$_2$O$_4$ and CuO$_6$ units, respectively.

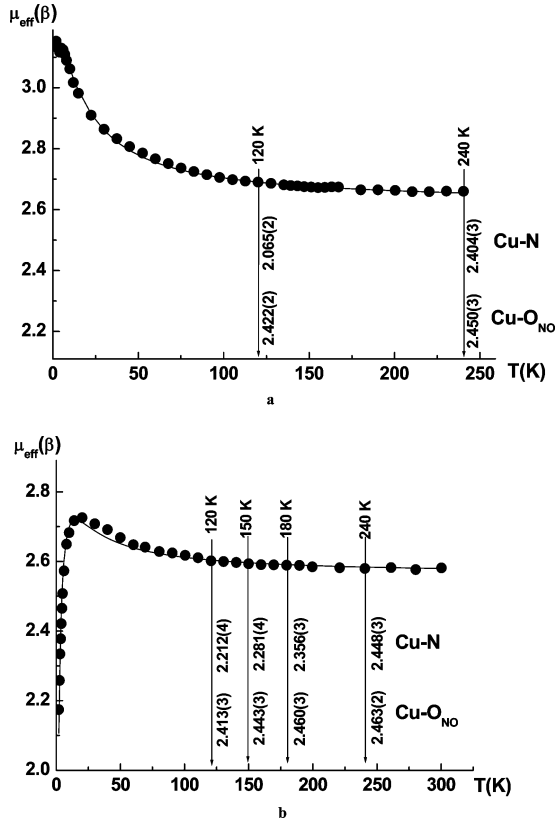

Figure 11. Temperature dependences of the effective magnetic moment of β-Cu(hfac)$_2$L·0.5C$_5$H$_{12}$ (a) and Cu(hfac)$_2$L·0.5Et$_2$O (b). Theoretical curves are shown by the solid lines. The vertical arrows indicate the temperature of the X-ray diffraction experiment; the upper and lower lines of the figures correspond to the Cu−N and Cu−O$_{NO}$ bond lengths in the CuN$_2$O$_4$ and CuO$_6$ units, respectively.

Indeed, our experiments showed that for amyl chloride and bromide solvates the experimental $\mu_{eff}(T)$ dependences proved very similar to the dependence for the hexane solvate (Figure 13). The abrupt change in μ_{eff} occurs in a narrow temperature range for all three solvates, namely, in the range 161 ± 3 K for Cu(hfac)$_2$L·0.5C$_6$H$_{14}$ (for this solvate, Figure 13 gives the $\mu_{eff}(T)$ dependence for the sake of convenient

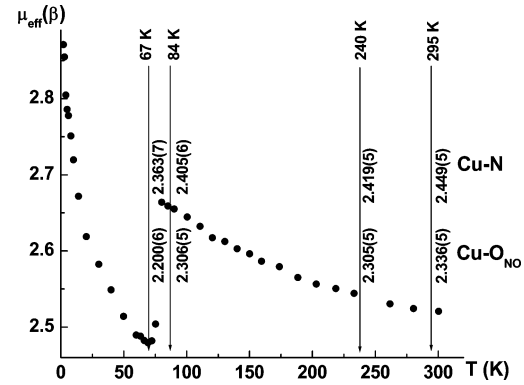

Figure 12. Temperature dependence of the effective magnetic moment of Cu(hfac)$_2$L (●).The vertical arrows indicate the temperature of the X-ray diffraction experiment; the upper line of the figure corresponds to the Cu−N bond lengths in the CuN$_2$O$_4$ units and the lower line to the Cu−O$_{NO}$ bond lengths in the CuO$_6$ units.

Chart 1

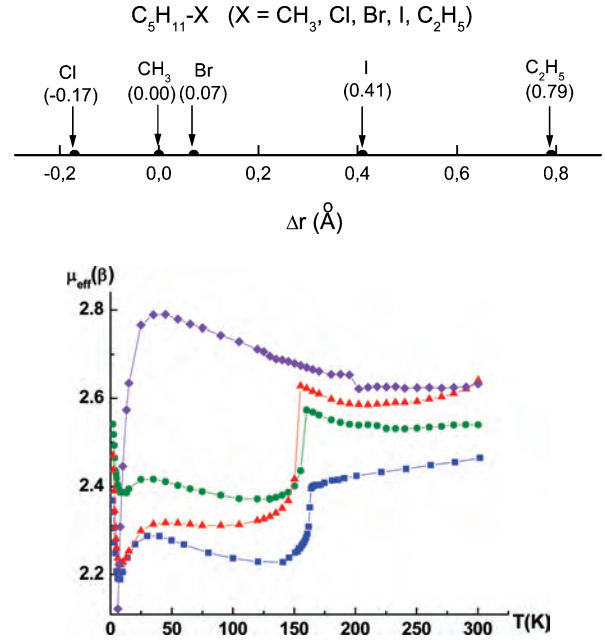

Figure 13. Temperature dependences of the effective magnetic moment of Cu(hfac)$_2$L·0.5C$_6$H$_{14}$ (blue squares), Cu(hfac)$_2$L·0.5C$_5$H$_{11}$Br (red triangles), Cu(hfac)$_2$L·0.5C$_5$H$_{11}$Cl (green circles), and Cu(hfac)$_2$L·0.5C$_5$H$_{11}$I (violet rhombs).

comparison), 155 ± 3 K for Cu(hfac)$_2$L·0.5C$_5$H$_{11}$Cl, and 150 ± 3 K for Cu(hfac)$_2$L·0.5C$_5$H$_{11}$Br. As in the case of Cu(hfac)$_2$L·0.5C$_6$H$_{14}$, this abrupt change corresponds to a drastic increase in the antiferromagnetic exchange interactions in half of all >N−•O−Cu^{II}−O•−N< spin triads, which is accompanied by a drastic decrease in the effective spin of these triads to $^1/_2$.

The similarity of changes in the magnetic properties of the solvates is caused by the identity of the structural transition. To avoid repetitions for the experimental $\mu_{eff}(T)$ dependence with indications of the temperature sections for solvates with amyl chloride and bromide, we give their selected crystal and structural data in Table 2. These data show that, after the transition of the high-temperature polymorphic modification to the low-temperature form, the independent part of the structure and hence the unit cell

Table 2. Space Groups and Selected Bond Lengths for $Cu(hfac)_2L\cdot0.5C_5H_{11}Cl$, $Cu(hfac)_2L\cdot0.5C_5H_{11}Br$, and $Cu(hfac)_2L\cdot0.5C_5H_{11}I$

$Cu(hfac)_2L\cdot0.5C_5H_{11}Cl$							
T, K	125	145	170	185	200	240	295
space group	$P\bar{1}$				$P\bar{1}$		
Z	4				2		
$Cu-O_{NO}$	2.344(3) 2.002(3)	2.346(2) 2.030(3)	2.312(2)	2.297(2)	2.301(2)	2.310(3)	2.316(2)
Cu−N	2.438(4) 2.452(4)	2.443(3) 2.458(3)	2.469(2)	2.468(2)	2.480(2)	2.501(3)	2.511(2)

$Cu(hfac)_2L\cdot0.5C_5H_{11}Br$						
T, K	100	165	175	200	240	295
space group	$P\bar{1}$			$P\bar{1}$		
Z	4			2		
$Cu-O_{NO}$	2.362(2) 2.004(2)	2.341(2)	2.324(2)	2.310(2)	2.320(3)	2.335(4)
Cu−N	2.445(2) 2.481(2)	2.479(3)	2.477(2)	2.483(3)	2.514(3)	2.530(4)

$Cu(hfac)_2L\cdot0.5C_5H_{11}I$					
T, K	100	190	205	240	295
space group,			$P\bar{1}$		
Z			2		
$Cu-O_{NO}$	2.376(2)	2.327(3)	2.329(3)	2.336(3)	2.345(3)
Cu−N	2.445(2)	2.483(3)	2.489(3)	2.512(3)	2.531(3)

volume are doubled. The CuN_2O_4 unit in $Cu(hfac)_2L\cdot0.5C_5H_{11}Cl$ and $Cu(hfac)_2L\cdot0.5C_5H_{11}Br$ become pseudocentrosymmetric because the Cu−N distances become different. As in the case of the transition to the low-temperature $Cu(hfac)_2L\cdot0.5C_6H_{14}$ phase, the CuO_6 units remain centrosymmetric, but form units of two types. In one of these groups, the axial $Cu-O_{NO}$ distances noticeably increase [2.312(2) → 2.344(3) Å in $Cu(hfac)_2L\cdot0.5C_5H_{11}Cl$ and 2.341(2) → 2.362(2) Å in $Cu(hfac)_2L\cdot0.5C_5H_{11}Br$]. In the other, the $Cu-O_{NO}$ distances are drastically shortened [2.312(2) → 2.002(3) Å in $Cu(hfac)_2L\cdot0.5C_5H_{11}Cl$ and 2.341(2) → 2.004(2) Å in $Cu(hfac)_2L\cdot0.5C_5H_{11}Br$; Table 2]; as a result, the O_{NO} atoms in these units pass to the equatorial positions, and two O_{hfac} atoms are displaced to the axial positions ($Cu-O_{hfac}$ ~2.0 → 2.2 Å). The dramatic shortening of the $Cu-O_{NO}$ distances in half of all $>N-^{\bullet}O-Cu^{II}-O^{\bullet}-N<$ exchange clusters, resulting from the structural rearrangement, causes strong antiferromagnetic exchange in them and, as a consequence, an abrupt decrease in μ_{eff}. Thus, the abrupt change observed on the $\mu_{eff}(T)$ curves for $Cu(hfac)_2L\cdot0.5C_5H_{11}Cl$ and $Cu(hfac)_2L\cdot0.5C_5H_{11}Br$ completely correlates with the structure dynamics of the complexes from high to low temperatures.

The only difference between the experimental $\mu_{eff}(T)$ dependences for $Cu(hfac)_2L\cdot0.5C_5H_{11}Cl$ and $Cu(hfac)_2L\cdot0.5C_5H_{11}Br$ and the dependence for $Cu(hfac)_2L\cdot0.5C_6H_{14}$ is the fact that when the temperature is lowered, the $Cu-O_{NO}$ distances start to increase after the shortening before the transition (Table 2), whereas in solid $Cu(hfac)_2L\cdot0.5C_6H_{14}$, they smoothly decrease (Figure 6). This is responsible for the dominant ferromagnetic exchange interaction inside $>N-^{\bullet}O-Cu^{II}-O^{\bullet}-N<$ spin triads in $Cu(hfac)_2L\cdot0.5C_5H_{11}Cl$ and $Cu(hfac)_2L\cdot0.5C_5H_{11}Br$ before the transition and for the gradual increase in μ_{eff} (in contrast to $Cu(hfac)_2L\cdot0.5C_6H_{14}$; Figure 13).

In solid $Cu(hfac)_2L\cdot0.5C_5H_{11}I$, the dominant tendency is the lengthening of the $Cu-O_{NO}$ bond after the transition. Therefore, the abrupt change in μ_{eff} for this compound differs from that for the compounds discussed above; the same relates to the character of the $\mu_{eff}(T)$ dependence. When the temperature is lowered from 295 to 100 K, the Cu−N distances in $Cu(hfac)_2L\cdot0.5C_5H_{11}I$ gradually decrease by ~0.09 Å; after the transition at 197 ± 4 K, the $Cu-O_{NO}$ distances, which initially slightly decreased, start to increase (Table 2). Because ferromagnetic exchange interaction inside $>N-^{\bullet}O-Cu^{II}-O^{\bullet}-N<$ spin triads become dominant after the structural transition (<197 K) in this compound, this leads to a slight abrupt increase in μ_{eff} at the transition temperature and its increase afterward.

Thus, our data show that the form of the $\mu_{eff}(T)$ dependence and the transition temperature is maintained if the hexane solvate molecules are replaced with the amyl chloride or bromide molecules; the amyl iodide and especially heptane solvate molecule are too large, which changes the form of the $\mu_{eff}(T)$ dependence.

When we found that the character of the magnetic effect was so sensitive to the size of the molecule, it became much easier for us to "reproduce" the form of the dependence and the transition temperature for α-$Cu(hfac)_2L\cdot0.5C_5H_{12}$ using butyl chloride, bromide, and iodide as solvents, which crystallized only as solids isostructural with α-$Cu(hfac)_2L\cdot0.5C_5H_{12}$ (Figure 9a). Indeed, as shown in Figure 14, the $\mu_{eff}(T)$ dependence differs only slightly in character among α-$Cu(hfac)_2L\cdot0.5C_5H_{12}$, $Cu(hfac)_2L\cdot0.5C_4H_9Br$, and $Cu(hfac)_2L\cdot0.5C_4H_9I$. However, $Cu(hfac)_2L\cdot0.5C_4H_9Cl$ was an exception from this series; this indicated that the structure of its solid phase differed from the structure of the other members of the series. Indeed, an analysis of the set of structural data showed that, in contrast to α-$Cu(hfac)_2L\cdot0.5C_5H_{12}$, $Cu(hfac)_2L\cdot0.5C_4H_9Br$, and $Cu(hfac)_2L\cdot0.5C_4H_9I$, in solid $Cu(hfac)_2L\cdot0.5C_4H_9Cl$ the solvate molecules were orientated in another way relative to the chains. In parts a and c of Figure 15, this is

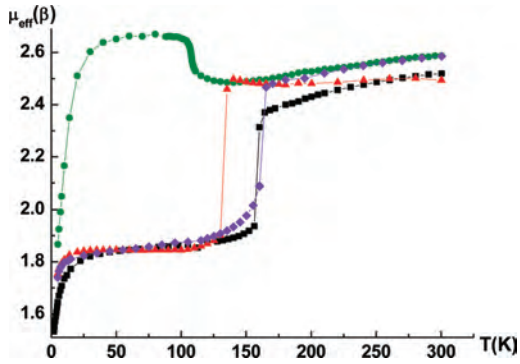

Figure 14. Temperature dependences of the effective magnetic moment of α-Cu(hfac)$_2$L·0.5C$_5$H$_{12}$ (black squares), Cu(hfac)$_2$L·0.5C$_4$H$_9$Cl (green circles), Cu(hfac)$_2$L·0.5C$_4$H$_9$Br (red triangles), and Cu(hfac)$_2$L·0.5C$_4$H$_9$I (violet rhombs).

illustrated (for easy perception) by the differently oriented double red arrows for the solvate molecules.

The arrangement of the solvate molecules depicted in the right part of Figure 15 indicates that the terminal atoms of the C$_4$H$_9$Br molecules (Figure 15d) are oriented in the cavities between the hfac fragment and the pyrazole ring of the CuN$_2$O$_4$ coordination unit. In the structure of Cu(hfac)$_2$L·0.5C$_4$H$_9$Cl (Figure 15b), the terminal atoms of the C$_4$H$_9$Cl molecules lie between the hfac fragment and the coordinated nitronyl nitroxide of the CuO$_6$ unit. This difference leads to the following. After the temperature-induced compression of the cavities that accommodate the C$_4$H$_9$Br or C$_4$H$_9$I molecules (Table 3), the solvate molecules exert pressure on the CuN$_2$O$_4$ units, thus provoking a rearrangement of the CuO$_6$ units. The specific orientation of the C$_4$H$_9$Cl molecules, however, hinders the structural rearrangement of the CuO$_6$ units (Table 3), and, after mild shortening, the Cu−O$_{NO}$ distances in the CuO$_6$ units again start to increase below 120 K.

Investigation of magnetostructural correlations inherent in the breathing crystals under study is important from the viewpoint of the classical approach, widely used in describing the exchange interactions in multispin systems in the framework of the Heisenberg−Dirac−Van Vleck model. Such a description is based on the data of magnetochemical experiment on the character of changes in magnetic susceptibility of the sample with temperature, which are analyzed using the corresponding spin Hamiltonian containing one or more exchange parameters (J_i). Importantly, it is assumed that J_i is almost temperature-independent.[18] The change in the exchange parameter was reported in few works, but when it was, it did not exceed 1 cm^{-1} in the order of magnitude.[19] Breathing crystals, however, represent a specific class of compounds in which the geometrical characteristics of the heterospin exchange clusters change significantly because of variation of the temperature. It is reasonable to assume that the J_i parameter is changed by the substantial spatial evolution of the {Cu^{II}−O$^{\bullet}$−N<} or {>N−$^{\bullet}$O−Cu^{II}−O$^{\bullet}$−N<} exchange clusters during the structural phase transition. This effect was investigated by electron paramagnetic resonance spectroscopy for Cu(hfac)$_2$L·0.5C$_8$H$_{18}$ crystals,[1m] and, indeed, it was found that J_i exhibited a strong temperature dependence. However, the dependence was reliably detected only in the region of the phase transition. Apart from the phase transition, the high error of experimental data dithered the $J_i(T)$ curve that did not allow us to determine the mechanism of the new (low- or high-temperature) phase formation. We succeeded in a quantum-chemical explanation of the $J_i(T)$ dependence.

For instance, for Cu(hfac)$_2$L·0.5C$_8$H$_{18}$ for which the structural rearrangement of the exchange clusters due to variation of the temperature is shown in Figure 4SI in the Supporting Information, it can be seen that above the transition point when the temperature decreases from 295 to 175 K, the Cu−O$_{NO}$ distances slightly decrease. As shown by quantum-chemical data, this leads to a slight increase in the efficiency of the exchange interaction in the copper-radical channel without changing the sign (Figure 16). The drastic shortening of the Cu−O$_{NO}$ distance in the region of the transition is according to the calculated data accompanied not only by a substantial change in the efficiency of the corresponding exchange interaction channel but also by sign reversal.

The values of J(CuL) calculated for seven different temperatures were used further for reconstructing the experimental dependence $\mu_{eff}(T)$ for Cu(hfac)$_2$L·0.5C$_8$H$_{18}$. For this, we used the procedure for calculating the temperature dependence of the effective magnetic moment described elsewhere[11,12] (the g factor was set at 2 for all paramagnetic centers). The resulting temperature curve of the effective magnetic moment for Cu(hfac)$_2$L·0.5C$_8$H$_{18}$ is shown in Figure 4 by the red lines connecting the calculated values of μ_{eff}. As can be seen, there is a good agreement between the experimental and reconstructed curves of $\mu_{eff}(T)$. Therefore, the reconstruction model of $\mu_{eff}(T)$ and the calculation procedure chosen are quite correct, and the >N−$^{\bullet}$O−Cu^{II}−O$^{\bullet}$−N< exchange clusters are sufficiently isolated in the solid. Note that the experimentally observed decrease in the magnetic moment with a decrease in the temperature from 295 to 175 K cannot be explained by X-ray diffraction data but is the result of the gradual increase of the low-temperature phase fraction in the high-temperature phase. In Figure 4 (and Figure 4SI in the Supporting Information), the X-ray data in the range ∼175−150 K (marked by a golden rectangle in Figure 16) do not correspond to the real shortening of the distances; rather, they correspond to the result of an averaging of the long Cu−O$_{NO}$ bonds inherent in the high-temperature phase and the short Cu−O$_{NO}$ bonds inherent in the low-temperature phase. That is, in the range 175−150 K, regions of the low-temperature phase (containing short Cu−O$_{NO}$ distances in its structure) gradually appear in the high-temperature phase, and a solid solution of the low-temperature phase is formed within the high-temperature phase. On the experimental $\mu_{eff}(T)$ curve, this manifests itself as the reduced value of the effective magnetic moment. After a certain critical content of the low-temperature phase, the rest of the high-temperature phase starts to transform into

(18) (a) Kahn, O. *Molecular Magnetism*; VCH: New York, 1993. (b) Carlin, R. L. *Magnetochemistry*; Springer-Verlag: Berlin, 1986.
(19) Kennedy, T. A.; Choh, S. H.; Seidel, G. *Phys. Rev. B* **1970**, *2*, 3645–3651.

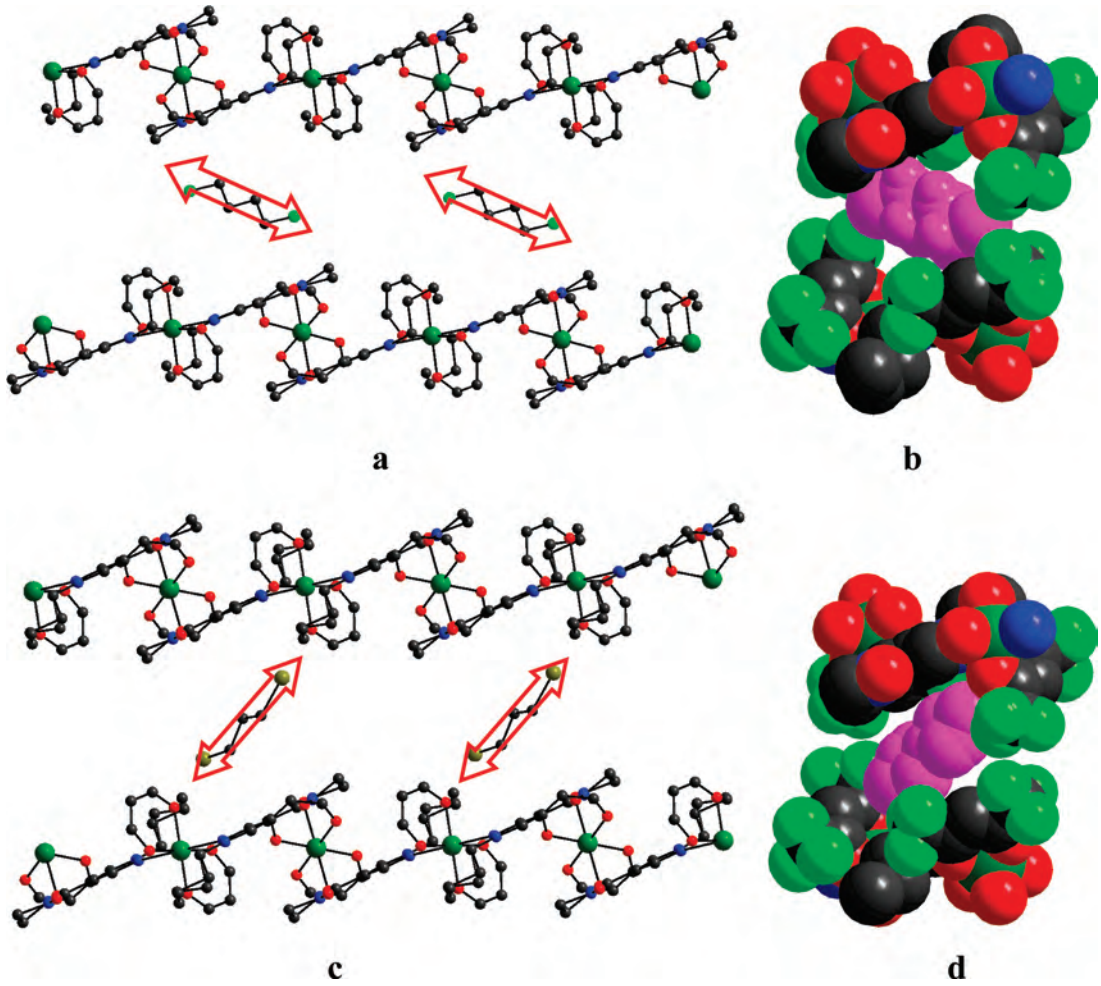

Figure 15. Different orientations of solvent molecules in the interchain space of $Cu(hfac)_2L\cdot 0.5C_4H_9Cl$ (a and b) and $Cu(hfac)_2L\cdot 0.5C_4H_9Br$ (c and d). On drawings a and c, the solvent molecules are enclosed in double red arrows; on drawings b and d, they are magenta-colored.

Table 3. Selected Bond Lengths for $Cu(hfac)_2L\cdot 0.5C_4H_9Cl$, $Cu(hfac)_2L\cdot 0.5C_4H_9Br$, and $Cu(hfac)_2L\cdot 0.5C_4H_9I$

			$Cu(hfac)_2L\cdot 0.5C_4H_9Cl$		
T, K	30	80	120	240	295
$Cu-O_{NO}$	2.382(2)	2.360(2)	2.275(3)	2.296(3)	2.315(5)
Cu−N	2.500(2)	2.483(3)	2.461(3)	2.481(3)	2.512(6)

		$Cu(hfac)_2L\cdot 0.5C_4H_9Br$		
T, K	105[a]	136	240	295
$Cu-O_{NO}$		2.270(3)	2.293(2)	2.318(6)
Cu−N		2.458(4)	2.491(2)	2.510(6)

		$Cu(hfac)_2L\cdot 0.5C_4H_9I$		
T, K	110	170	240	295
$Cu-O_{NO}$	2.004(2)	2.242(4)	2.302(3)	2.325(2)
Cu−N	2.461(3)	2.470(4)	2.495(3)	2.509(2)

[a] Crystal cracking.

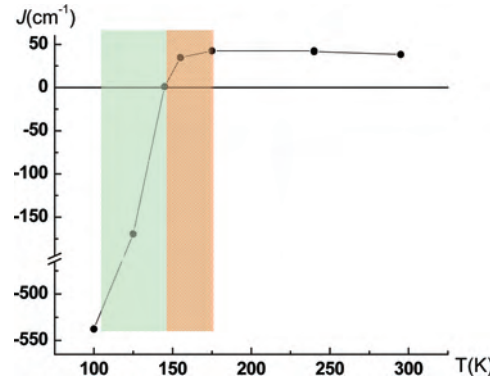

Figure 16. Temperature dependence of the intracluster exchange interaction parameter *J*(CuL) of $Cu(hfac)_2L\cdot 0.5C_8H_{18}$ (PBE0-calculated data).

the low-temperature phase in the range ~150−100 K (marked by a light-green rectangle in Figure 16). Here, indeed, all other long $Cu-O_{NO}$ distances decrease, which naturally leads to great changes in the exchange parameter (Figure 16). The same description of the phase transition is valid for the reverse transition from the low- to high-temperature phase. Therefore, the theoretical description gives rise to a more abrupt change on the $\mu_{eff}(T)$ curve in Figure 4, while the experimental curve is much smoother than the theoretical one obtained by analyzing the evolution of the exchange parameter.

As was pointed out above, for solvates with hexane and its spatial analogues, the independent part of the structure is doubled at the moment of the structural phase transition; the $Cu-O_{NO}$ distances are drastically shortened in half of all CuO_6 units and lengthened in the other half. The dramatic changes in the structural parameters also lead to an abrupt change on the $\mu_{eff}(T)$ curve (Figure 13). This is confirmed by the calculated exchange interaction parameters (Figure 17). For hexane and amyl bromide solvates in which the above-described transition takes place, the *J*(CuL) exchange coupling parameter abruptly changes from ferromagnetic to

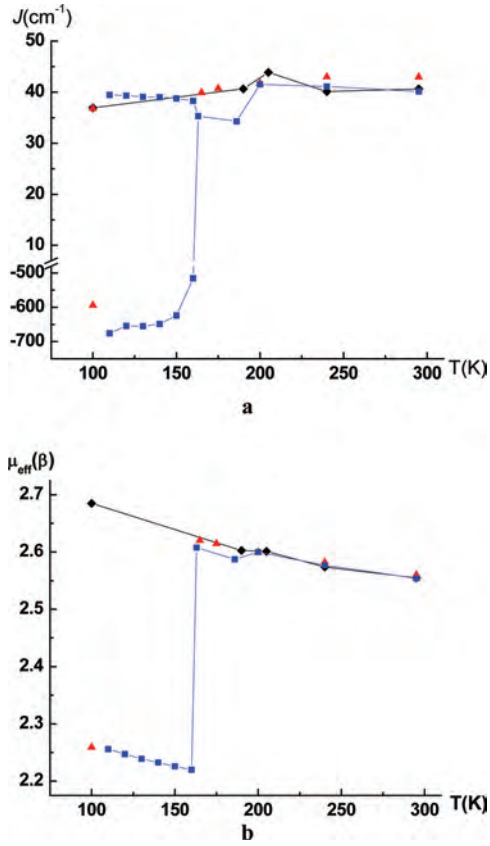

Figure 17. Calculated temperature dependences of the exchange interaction parameter J(CuL) (a) and effective magnetic moment (b) of Cu(hfac)$_2$L·0.5C_6H_{14} (blue squares), Cu(hfac)$_2$L·0.5C_5H_{11}I (black rhombs), and Cu(hfac)$_2$L·0.5C_5H_{11}Br (red triangles).

strongly antiferromagnetic at the transition temperature in half of all {>N−•O−Cu^{II}−O•−N<} exchange clusters. In the other half of exchange clusters, as well as in the case of the amyl iodide solvate, J(CuL) remains ferromagnetic and changes insignificantly with temperature. Note again that, according to quantum-chemical data, cooling to a temperature near the transition point leads to a gradual increase in μ_{eff} for Cu(hfac)$_2$L·0.5C_6H_{14} (Figure 17), while the experimental $\mu_{eff}(T)$ curve (Figure 13) shows some decrease in the effective magnetic moment in this region. This is related to the generation of the low-temperature phase regions in the high-temperature phase, for which lower values of μ_{eff} are characteristic.

Conclusions

X-ray and magnetochemical investigations of a series of synthesized Cu(hfac)$_2$L·0.5Solv chain−polymer complexes with incapsulated solvent molecules showed that the complexes are characterized by high intracrystal mobility with temperature. The structural changes occur mostly within the >N−•O−Cu^{II}−O•−N< heterospin exchange clusters. The lengthening or shortening of the Cu−O_{NO} bonds is accompanied by the mutually coherent shortening or lengthening of two Cu−O_{hfac} bonds along one of the orthogonal axes in the CuO_6 units. While changing in structure, the polymer heterospin chains "glide" over the solvent molecules as if the latter were inner hinges, which, in turn, make coherent motions correlated with the deformation of the CuO_6 units. This ensures the mechanical stability of the crystals, which do not destroy during the repeated heating−cooling cycles, providing one a rare opportunity to explore the crystal structure of the compound in the whole set of temperatures above and below the observed magnetic anomaly. Sequential representation of the structure using the temperature as the fourth coordinate permits one to visualize for the first time the sophisticated set of correlated intracrystalline motions, i.e., actually to represent structural transformations of the complex as a movie (Supporting Information). These movies provide direct support for the cooperative character of the observed phenomenon.

Because solvent molecules take an active role in mutually correlated intracrystalline motions, they have a substantial indirect effect on the rearrangement of the coordination units containing >N−•O−Cu^{II}−O•−N< exchange clusters and, hence, on the temperature T_a and the character of the magnetic anomaly on the $\mu_{eff}(T)$ curve (see Table 1). The effect of the solvent inclusion on the magnetic anomaly of Cu(hfac)$_2$L·0.5Solv proved so substantial that typical modification of the included solvent molecules by the addition of one methylene unit was in this case exceedingly large in its effect on the structural "chemical step". The magnetic effects under study can be strongly affected even by the substitution of the C−C single bond by the C=C double bond (octane and octene). In their effect on the character of the magnetic anomaly, such variations of solvate molecules are comparable to substitution of the alkyl substituents directly in the pyrazole ring of the nitronyl nitroxide.[1f−i]

Because the development of approaches to *chemical control* over the character and temperature of the physical effect demands predictability of the results, we considered a smaller structural step. For the series Cu(hfac)$_2$L·0.5C_6H_{14} ↔ Cu(hfac)$_2$L·0.5C_5H_{11}Cl ↔ Cu(hfac)$_2$L·0.5C_5H_{11}Br ↔ Cu(hfac)$_2$L·0.5C_5H_{11}I and α-Cu(hfac)$_2$L·0.5C_5H_{12} ↔ Cu(hfac)$_2$L·0.5C_4H_9Cl ↔ Cu(hfac)$_2$L·0.5C_4H_9Br ↔ Cu(hfac)$_2$L·0.5C_4H_9I, we actually tested a more gentle approach, which allowed us to trace the transformation of the magnetic properties with minor changes in the linear dimensions and flexibility of the varied solvate molecules. This approach proved successful. However, even in these series (hexane−amyl chloride−amyl bromide and pentane−butyl bromide−butyl iodide), where there were no electronic or polarization effects, the difference in the transition temperature was pronounced (Figures 13 and 14). For solvates with amyl iodide (Figure 13) and butyl chloride (Figure 14), the transformation of the $\mu_{eff}(T)$ curve was more significant and showed that the crystal packing of the compound was sensitive even to minor changes. Variation of the spatial characteristics within these series allows one to determine the range of solvates in which the magnetic anomaly retains its form, while T_a changes insignificantly.

The specific behavior of the experimental $\mu_{eff}(T)$ curve, which is often observed with a change in the temperature down to the phase transition point, should also be noted. As shown by quantum-chemical study, the experimentally observed decrease in the magnetic moment is the result of

the gradual increase in the fraction of the low-temperature phase in the high-temperature phase, although the J parameter changes insignificantly before the transition temperature is reached. Substantial changes in the exchange parameter take place in the vicinity of T_a and concern both its magnitude and sign.

To summarize, the results obtained show that the problem of chemical control over the physical characteristics of the spin transition in heterospin solvates can be solved by varying the solvent inclusion using at first a "rough structural step" and then a "gentle structural step"; in this way, one can obtain solids with any specified transition temperature. For the compounds discussed in this work, T_a can be varied within the range $\sim$50−200 K. On the basis of Cu^{II} heterospin complexes with nitroxides, one can obtain compounds with T_a on the order of room temperature and above, and such compounds already exist.[1] If they are found capable of including solvent molecules, they will certainly be liable to fine adjustment of T_a by selective variation of the solvate molecules. There are still a number of open questions that should be clarified in further studies; among them are the origin of abrupt or gradual character of magnetic anomalies, as well as the reasons why in some of the solvates the structural rearrangement takes place in only a half of the CuO_6 coordination units, leading to a change of μ_{eff} that corresponds to the disappearance of one-fourth of the paramagnetic centers in the system. The careful examination of intermolecular contacts is needed to figure out those playing a crucial role in the course of structural and magnetic transition. This, as well as heat capacity and pressure effect studies, will be the subject of future work.

Acknowledgment. This work was supported by RFBR (Grants 06-03-32157, 06-03-32742, 09-03-00091, and 08-03-00025), President of Russia Grants (NSh-1213.2008.03 and MK-2030.2008.3), CRDF (Grant RUE1-2839-NO-06), RAS, and SB RAS.

Supporting Information Available: Structural determination parameters, crystal and structure refinement data, atomic coordinates, and isotropic displacement parameters for all complexes (in CIF format); X-ray movies for solvates with hexane and heptane; Figures 3SI, 4SI, and 9SI; and complete ref 7. This material is available free of charge via Internet at http://pubs.acs.org.

IC8011074